Relaxation Behavior in Molecular Dynamics Simulations of Simple Polymers

Taylor Dotson

May 1, 2008

Abstract

Viscoelastic materials exhibit complex stress-strain behavior with respect to time, temperature and magnitude. Study of viscoelastic behavior by physical experimentation is very much limited by the cost and current capabilities of rheological equipment. Additionally, macroscopic relaxations often occur at time-scales that are impractical to study experimentally. For this reason, computer molecular dynamic simulations are becoming increasingly popular in this field of study. Mechanical behavior on the molecular level can be studied through the use of autocorrelation functions with the intention of using them to eventually predict the macroscopic stress relaxation modulus of the given material. However, the inversion of such functions into a useful model tends to be a very ill-posed problem and many widely used inversion methods do not adequately address this ill-posedness. Mechanical relaxation is explored on a microscopic level through the use of autocorrelation functions for several simple bead-spring models of short polymer chains. Specifically, the end-to-end and dihedral angle correlation functions are analyzed. The parameters are found to collapse to single-valued functions for the freely jointed and freely rotating models.

Contents

List of Figures

1 Introduction

A glassy material is one which exhibits the properties of a normal solid at very low temperatures but lacks a defined crystal structure. That is, it is an amorphous or disordered solid. However, glasses are not completely disordered, as one would see in a gas. Rather they only display short-range order as opposed to the long-range order seen in crystalline solids [28]. Thus, as its degree of order resembles that of a liquid, it can be questioned whether a glass is a true solid or just a super-cooled liquid [89]. Mechanical behavior of glassy materials is generally much more complicated than that of normal crystalline solids and, because such materials constitute much of our man-made world, the understanding of this behavior is the subject of a great deal of research. There remain many unanswered questions in glass research.

Much of the confusion about glassy materials stems from the incredible time scales with which they deform and change. A popular myth about window glass, for example, states that very old window glass is thicker at its base due to the glass flowing with time. In fact, the old glass panes are thicker at the bottom because the techniques used in manufacture did not yield uniform thickness and clearly the builder would mount the panes with the thick side down for practical reasons [82]. Theoretical estimates of the flow time of glass have shown that a result consistent with the one stated in the myth would have to occur over a time period much longer than human history [90]. Thus, it becomes clear that one cannot practically perform experiments to study behavior that occurs over such long time-scales. For this reason, much work is performed in the field in search of greater understanding of the molecular basis of long-term changes in glassy materials. In this paper we attempt to contribute to this understanding through molecular level simulation of simplified polymer chains.

1.1 Mechanical Properties

1.1.1 Viscosity and Modulus

One property of most glassy materials is that they exhibit viscoelastic behavior over some wide range of temperatures. The various moduli that describe the mechanical response of the material are, generally, time dependent. A

notable example is stress relaxation. If one were to attempt to apply a finite strain (deformation) to an elastic material, one would encounter a constant resistive stress proportional to the strain (i.e. Hooke's Law). The ratio of this stress to the applied strain is constant with respect to time for a given material and state point and is called the modulus. Additionally, the mechanical properties of a Newtonian liquid is described through the ratio of the resistive stress with the applied strain rate which is called the viscosity of the liquid. As a result, one can model an elastic solid as an ideal spring while a liquid can be modeled as an ideal dashpot.

However, in a viscoelastic material, one finds both elastic solid-like and liquid-like behavior. The resulting mechanical behavior can be modeled as a combination of springs and dashpots [29]. The stress-strain relationship is much more complicated for such a material and is given by equation (1):

$$\sigma(t) = \int_0^t G(t-s)\,\dot{\gamma}(s)\,ds \tag{1}$$

where G is the time dependent relaxation modulus of the material, σ is stress and $\dot{\gamma}$ is the strain rate [29].

Anyone who has dealt with systems of springs and dashpots knows that such a system has an associated decay curve when perturbed. Such decay curves are of interest experimentally and one can obtain one through a stress-relaxation experiment.

If one were to apply a small constant strain to a viscoelastic material, one would encounter a resistive stress that slowly decays (i.e. relaxes) to zero. The time for this stress to decay characterizes the stress-relaxation time-scale of the material. The fact that this force decays to zero reflects the material's inability to store elastic energy over very long times. This is due to the partially liquid like characteristics of the material which cause it to dissipate mechanical energy by deforming non-elastically. Essentially, the material makes configuration adaptations on the molecular level in order to adjust to its newly imposed shape. Through this mechanism it is said the material loses its "memory" of its original shape. One can easily measure $G(t)$ on the macroscopic level through such stress-relaxation experiments. It is clear that if $\gamma(t)$ takes the form of a step function at s=0, then the strain

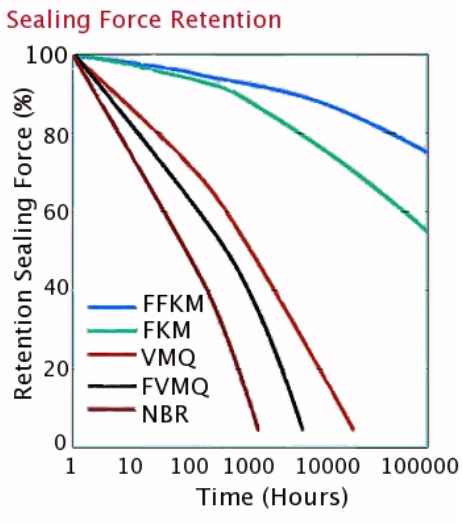

Figure 1: Stress Relaxation Data [39].

rate (velocity of deformation) is approximately a delta function at time zero. Thus, equation (1) reduces to:

$$\sigma(t) = \gamma(0)\, G(t) \tag{2}$$

That is, the measured stress is proportional to the time-dependent modulus.

Figure 1 displays the results of compressive stress relaxation tests for various elastomeric o-rings. In this test the percent sealing force retention is equivalent to the modulus. Such testing is very important to scientists and engineers. For example, one of many factors that caused the Challenger disaster was that booster rocket o-rings became non-pliable (i.e. took a long time adjust to shape changes) and did not seal correctly in the low morning temperatures [73].

It is very often useful to describe G in the frequency domain by performing a one sided Fourier transform on $G(t)$ producing a real storage modulus, $G(\omega)'$, and an imaginary loss modulus, $G(\omega)''$. The storage modulus strictly describes the elastic or energy storing behavior of the material while the loss modulus instead describes the liquid-like or energy dissipating behavior.

The reason why this is so is clear when considering dynamic experiments in frequency space. To perform a dynamic modulus test, for example, one applies an oscillating shear strain to the sample and observes the magnitude and phase angle of the resulting stress.
From such an experiment one obtains a complex modulus:

$$G^{*}(\omega) = G(\omega)' + \imath G(\omega)'' \tag{3}$$

by using the following relationship:

$$\sigma(t) = \gamma^{0}\left(G' \sin \omega t + G'' \cos \omega t\right) \tag{4}$$

where γ^{0} is the amplitude of the applied sinusoidal strain. Given that in a purely elastic material response displacement is always in phase with the applied force while a viscous response is always 90 degrees out of phase with the oscillating driving force,[29] it becomes clear that Fourier sine and cosine components of the transform provide the loss and storage modulus respectively. The division of the modulus into energy storing and dissipating frequency dependent constituents also provides additional information about the mechanical properties of the material as discussed below. The exact relationships is shown in equation (5).

$$G'(\omega) = \omega \int_{0}^{\infty} G(s) \sin \omega s ds \qquad G''(\omega) = \omega \int_{0}^{\infty} G(s) \cos \omega s ds \tag{5}$$

An example of dynamic moduli is shown in Figure 2.

The driving frequency of the experiment is directly related to the shear rate. For a given driving amplitude (i.e. maximum shear) an increase in driving frequency results thus results in the shear being applied over a shorter time period and thus exposes the material to higher shear rates. The shear rate plays an important rule in the mechanical response of a viscoelastic material. For example, silly-putty easily stretches or 'flows' like a liquid for small shear rates while it shatters like window glass when subjected to a violent shock (Figure 3). That is, the ability of silly-putty to dissipate energy at large strain rates (i.e. high frequencies) is relatively weak.

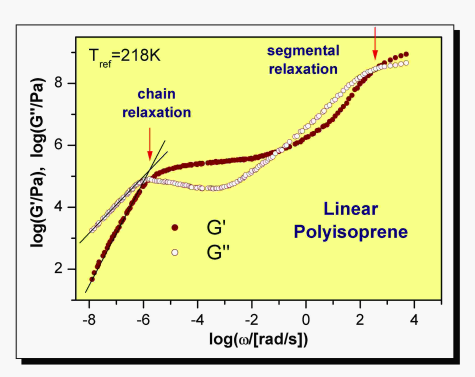

Figure 2: Dynamic Relaxation Moduli in pascals (N/m^2) [65]

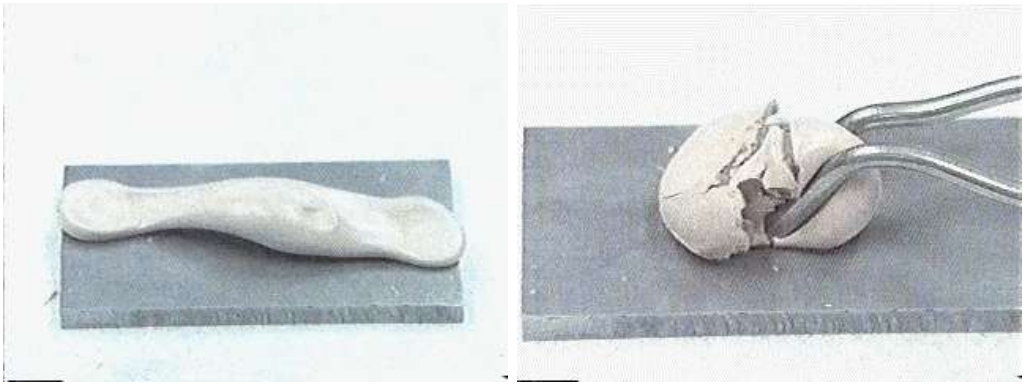

Figure 3: Top:Silly Putty Under Small Strain Rates. Bottom: Silly Putty Under Large Strain Rates [23]

In dielectric spectroscopy experiments one takes a polar viscoelastic material and observes its polarization with regard to an external sinusoidally varying electric field. Such experiments are similar to capacitance testing. The imposed electric field is of a known form but the measured field in the material will differ from the imposed field in a way depending on the properties of that material. The measurements will lag and differ in magnitude from the driving field as a result of the energy needed to reorient the average dipole of the material. Watching the phase behavior of the dipole with switching frequency one can obtain a complex permittivity, $\epsilon^*(\omega)$, which should be comparable to the macroscopic modulus since the movement of the dipoles is determined by their local viscous environments and the overall material

response is thought to be based on configurational changes on the molecular level. The equations governing these experiments are the same as those of the dynamic modulus testing listed above. However, experimental result have been contradictory [1, 22, 61]. The shapes of the macroscopic and microscopic frequency based relaxation spectra have not been found to coincide in every case. The analysis of relaxation functions is expounded on in a later section.

1.1.2 The Debye Model

Dielectric spectroscopy is of particular interest because of the existence of a particularly useful model of dielectric relaxation: the Debye Model. The Debye Model begins with the assumption that the molecule being rotated by the external field can be approximated by a rigid rod. In addition, it is assumed that the environment of the molecule can be modeled as a uniform frictional bath. Carrying through the analysis of the model [25] one finds the complex permittivity to be described by the following function:

$$\epsilon^* (\omega) = \frac{1}{1 + \imath\omega\tau} \tag{6}$$

and the equivalent time domain relaxation function is a single exponential:

$$\phi (t) = e^{-t/\tau} \tag{7}$$

While this model is useful, the majority of materials are not well described by the equations of the Debye Model. That is, they display varying degrees of non-Debye behavior.

1.1.3 Non-Debye Relaxation Functions

To make physical statements about either time or frequency dependent moduli one must fit them to functional forms. This can be tricky, especially for the frequency dependent data. The time dependent stress relaxation modulus is often fit by a stretched exponential or Kohlrausch-Williams-Watts (KWW) function as it's called in the literature [44].

$$G(t) = Ae^{-\left(\frac{t}{\tau_{KWW}}\right)^{\beta_{KWW}}} \tag{8}$$

The frequency dependent data is often fit using a Cole-Davidson (CD) function (9) [24].

$$\frac{G^*(\omega) - G_\infty}{G_0 - G_\infty} = G'(\omega) - \imath G''(\omega) = \left(\frac{1}{1 + \imath\omega\tau_{CD}}\right)^{\beta_{CD}} \tag{9}$$

It is worth noting that both the KWW and the CD functions are simply the Debye formulas above with the addition of the exponent, $0 \leq \beta \leq 1$, which marks the degree of non-Debye behavior. However, these functions are in no way equivalent, that is, they are not Fourier transform pairs.

1.1.4 Time-Temperature Superposition

Most experimental set-ups are only useful for limited ranges of frequency or time. Therefore one needs to piece together data from different experiments to create a set of master curves of material properties over several orders of magnitude (e.g. viscosity-temperature curves). However, in order to do this, one must make certain physical assumptions. One assumes Time-Temperature Superposition (TTS) [80]. TTS states that for viscoelastic material time and temperature are essentially equivalent for a given material [29]. That is, one can determine long time behavior of the relaxation modulus by performing the experiment at lower temperature and vice-versa. When using TTS one is assuming that if the entire experiment were possible at a single temperature, the resulting modulus curve would be the same as the curve composed of the superposition of many different experiments. It is a useful property to utilize when fitting various models. A material for which TTS is found to be valid is called rheologically simple. However, it has been observed that TTS ceases to hold true as one approaches the glass transition temperature in polymers [68, 79]. Thus one must be careful in one's application of TTS.

Once the assumption that TTS holds is made, the principal is not very difficult to apply. After obtaining experimental results at several different temperatures there are two shift factors one needs to overlay the data: a time

scale shift factor and a modulus scale shift factor, a_T and b_T respectively [76]. First, one chooses the reference temperature (T_o) and then calculates:

$$a_T = \frac{D\left(T_o\right)}{D\left(T\right)} \qquad b_T = \frac{\rho T}{\rho_o T_o} \tag{10}$$

for each experimental temperature where D is the diffusion coefficient and ρ is the density. Application to the complex modulus G^* produces [76]:

$$G^*\left(\omega, T\right) = b_T G^*\left(\omega a_T, T_o\right) \tag{11}$$

The final result should be a graph like figure 4:

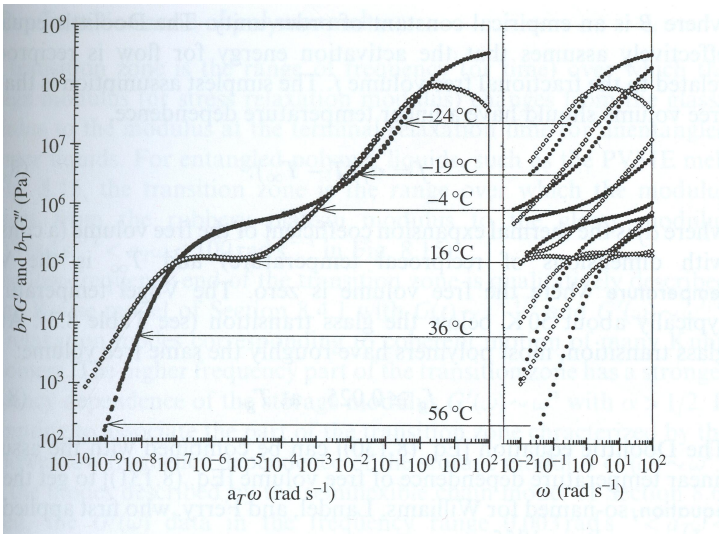

Figure 4: Application of TTS producing frequency dependent moduli master curves [76]

Similarly, one finds [76]:

$$G\left(t, T\right) = b_T G\left(t/a_T, T_0\right) \tag{12}$$

The derivation of these results is relatively straightforward in terms of the Rouse model. The Rouse model is simplified bead-spring model of polymer

chains. The most important implication of the model with regard to TTS is that all relaxation times change the same with respect to temperature. This model is discussed in more detail in a later section 3.1. Here only some important results of the model are necessary in demonstrating how the shift factors are obtained. A more detailed description can be found in [76].

First, the reciprocal of the diffusion coefficient of a material represents a kind of characteristic relaxation time at a given temperature.

$$\tau \sim \frac{1}{D(T)} \tag{13}$$

In addition, one can find that the modulus associated with this time to be related to the product of density and temperature.

$$G(\tau) \sim \rho T \tag{14}$$

The first result is obtained from relationship (14):

$$\frac{G(t_0, T_0)}{G(t, T)} \tag{15}$$

where T_0 is the reference temperature.
If one assumes that all relaxation times for the system change with temperature in the same manner as the characteristic relaxation time determined by the diffusion coefficient, we can use relationship (13) to relate the the differing time scales of the experiments.

$$\frac{t}{t_0} = \frac{D(T_0)}{D(T)} \tag{16}$$

Thus, using definition (10) results in:

$$G(t, T) = b_T G(t/a_T, T_0) \tag{17}$$

The frequency space result follows from the fact that time and frequency have reciprocal units. Thus the result for the complex modulus, G^*, is:

$$G^*(\omega, T) = b_T G^*(\omega a_T, T_0) \tag{18}$$

It is important to note that, in order for the above process to produce a smooth master curve, the functional form of the modulus curve must be the

same for different temperatures. However, since one cannot generally do a single experiment covering the full range of time it is easy to assume the functional form to be much simpler than it may actually be.

For example, in [77] stress relaxation moduli are determined for glycerol and is found to be reasonably well fit by stretched exponentials. The stretching parameter, β was found to vary with temperature. One may be inclined to state that this clearly demonstrates TTS is violated. The researchers, however, concluded that it was not necessarily a violation and continued to construct a master curve for glycerol. Their rational was that perhaps the master curve is not a stretched exponential but rather best described by a stretched exponential with a slowly varying stretching parameter.

This is not a claim to make without reasonable justification. From the above derivation, we know that if TTS applies than all relaxation times must change in the same way with regard to a given change in temperature. Thus we then must describe our modulus curve in terms of a spectrum $\rho(\tau)$:

$$G(t) = \int_0^\infty \rho(\tau)\, e^{-t/\tau} d\tau \tag{19}$$

It is this spectrum, $\rho(\tau)$, that must maintain its shape from one temperature to another and merely shift horizontally. Unfortunately, this spectrum is very difficult to obtain for a relaxation curve and impossible to determine with absolute certainty. This is explored further when spectral inversion methods are discussed.

As a result, the modulus curves are often described by useful but merely empirical functions, such as the KWW stretched exponential and Cole-Davidson (CD) functions, that often don't completely describe the modulus and/or lack theoretical justification. This poses several difficult questions if one finds the parameters of ones functional fits to change with temperature. Does this function really describe the decay? Does the change in the function's parameters truly reflect an alteration in the underlying relaxation spectrum or is it a result of an inappropriate fitting function?

The first difficulty with using the KWW or CD functions is a practical one. In general these functions do not follow the principle of TTS. To illustrate this point let's consider the two functions. Let us consider, for the sake

of simplicity, a fundamental relaxation coefficient of one. By TTS each relaxation experiment (performed at a different temperature) sees the same relaxation but a different scaling of time:

$$\phi(t)_1 = e^{-(t)^\beta} \tag{20}$$

$$\phi(t)_2 = e^{-(\alpha t)^\beta} \tag{21}$$

If a scaling factor of $a_T = 1/\alpha$ is introduced to the second equation then clearly ϕ_2 would be equivalent to ϕ_1. However if we assume that as a result of the change of temperature which caused the change of the decay constant the stretching exponent increased by some small amount δ then no simple scaling factor will force the second function to be equal to the first. This is made more clear by looking at the log transforms of these functions:

$$\log \phi(t)_1 = -t^\beta \tag{22}$$

$$\log \phi(t)_2 = -\gamma t^\beta t^\delta \tag{23}$$

where $\gamma = \alpha^{\beta+\delta}$. Clearly no scalar factor can make these two functions equal as each one dependents on time in a different manner.

The second difficulty is that empirical fits of data are inherently limited. The function will invariably fail to fit the data perfectly. As a result one can never be too sure if the physical significance of a change in parameter values. If the fit does not work over the entire range of data then a change of fitting parameters may not indicate a shift in the underlying physics but perhaps a change in the region best fit by the function being used. This issue will be addressed further in the results sections.

1.2 The Glass Transition

As was stated before, viscoelastic materials display properties of solids and liquids. In addition, it is not surprising that that these materials are essentially liquids at high temperatures. As is seen in figure 6, when the temperature is lowered the seemingly liquid viscoelastic material becomes more and

more viscous. The viscosity actually diverges to infinity at a nonzero temperature. This observation is important for several reasons. The viewpoint of viscosity as being the result of thermally activated processes would cause one to expect Arrhenius behavior of viscosity [76]:

$$\nu \sim \exp \frac{A}{T} \tag{24}$$

where A is a constant and T is temperature. That is, one would expect the viscosity to diverge at absolute zero. The actual behavior is instead empirically described by the Vogel-Fulcher equation [86, 30].

$$\nu \sim \exp \frac{A}{T - T_0} \tag{25}$$

The viscosity is observed to diverge at this nonzero temperature T_0. In addition, one sees the viscosity become so great at some nonzero temperature $T \geq T_0$ that the material is essentially a solid. For this reason one would reason that since there is a change in phase that there should exist some temperature $T_g \geq T_0$ where the behavior clearly transitions from that of a highly viscous liquid to that of a solid: the glass transition temperature.

The existence of the glass transition is an often debated topic in modern physics. Many polymers exhibit solid-like behavior at room temperature but lack the ordered molecular structure of common solids. In addition, many do not consider it to be a true phase transition because of the arbitrariness with which the transition temperature T_g is defined and the fact that it changes with cooling-rate. The glass-transition is often defined as the point when the viscosity of the substance becomes 10^{12} poise. Water, for comparison, has a viscosity of 10^{-2} poise.

An alternative definition is that T_g is the temperature at which the volume of a sample departs from its equilibrium volume for a given cooling rate [55]. Experimentally this is done by cooling a sample at a given rate to different temperatures and watching to see if the volume of the sample decays to an equilibrium level. A plot of this phenomena is shown in figure (5).

However, the consideration of the glass transition as a real phase transition is still controversial. Since there is no latent heat associated with the glass transition temperature or a discontinuity of thermodynamic property such

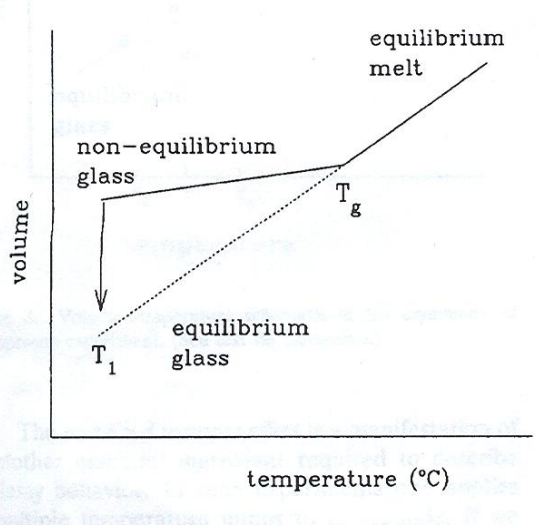

Figure 5: The glass transition temperature T_g [55]

as density or volume, the glass transition is not considered to be a first-order phase transition [89]. What one does see is a discontinuity in the slope of thermodynamic properties such as heat capacity or specific volume (as seen in figure (5)) [47] by which one would consider the glass transition to be a second order phase transition.

The temperature dependence of viscosity in glassy materials is generally shown through Angell plots (figure (6)) where one plots the log of viscosity versus T_g/T. One notes that there are two distinct behaviors in such a plot. There are materials whose behavior is linear on the Angell plot and those which show a divergence. Such materials are called strong and fragile glass formers, respectively. These labels come from old glassblowing terms. The viscosity of a material that shows linear behavior on an Angell plot clearly has a weaker temperature dependence as it cools and as a result it is much easier to obtain uniform cooling, hence they are strong glass formers. Fragile glass formers, on the other hand, exhibit drastic changes in viscosity for small changes in temperature at low temperatures which leads to weakness in the glass.

However, an Angell plot is sometimes not useful because the dependence of

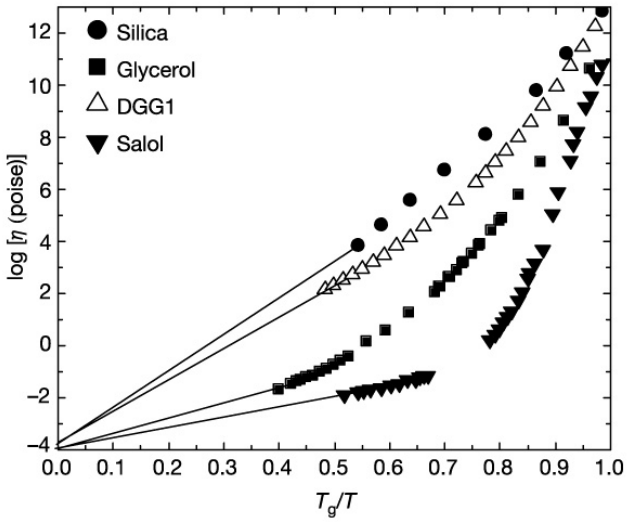

Figure 6: An Angell Plot for various glassy materials [62]

viscosity on pressure is ignored. If one were to plot viscosity data from different pressure experiments one would end up with a multi-valued function. Additionally, the exact value of T_g is questionable and one would like to create plots of material properties without having to accept the theoretical baggage of the glass transition. For these reasons, the search for a single suitable material parameter with which one obtains a single-valued function for a relaxation behavior, such as viscosity, has been an important area of research.

Such a suitable static material property is called a scalar metric. The idea is that the time-scale of relaxation behavior of a viscoelastic material can be completely described by a single variable property of the material (the scalar metric). The term scalar metric is used because the ability to describe the relaxation properties of the material by a single variable implies that this same variable represents a distance from the glass transition. It has been found that packing fraction, non-bonded energy density and the location of the first peak of the static structure factor all can serve as scalar metrics [18]. In addition, it has been found that the product $T^{-1}V^{-\gamma}$ can serve as a scalar metric where T is temperature, V is specific volume and γ is a system specific parameter [20]. Regardless of the temperature, pressure or density, when a type of relaxation time-scale for a series of simulations is plotted

versus one of these scalar metrics the the data collapses to a single valued curve. We will explore the scalar metric further after introducing the reader to molecular dynamics.

1.3 Molecular Dynamics

In the field of condensed matter physics there are two different ways of simulating systems of molecules: Monte-Carlo (MC) and Molecular Dynamics (MD). In Monte-Carlo simulations the next move of the molecule is randomly generating and has certain probability of being accepted or rejected by the code based on physical arguments for the system. MC simulations are useful for obtaining thermodynamic and configurational information and is clearly useful for Quantum level simulation. However, time is not clearly defined for these types of simulations.

In MD simulations, however, one defines the series of potentials (interatomic, bond, torsion, etc.) for the molecules, begins the simulation, and then integrates Newton's Laws to obtain particle trajectories. That is, the MD method is simplify the solving of a large system of differential equations. One additionally holds the simulation in a certain statistical mechanical ensemble such as constant number of particles, volume and temperature (NVT) or constant number of particles, pressure and temperature (NPT). The temperature is maintained through one of a variety of numerical thermostats [15, 32, 63] which achieve their goals through very different means and the details of which are beyond the scope of this paper. Given the additional limitations of computational ability one "fools" the simulated sample of atoms and molecules into thinking it is a constituent of a larger sample by applying periodic boundary conditions (see figure (7)) in which a particle leaving the right side of the box returns on the left. A useful introduction to molecular dynamics methods is provided by Allen and Tildesley [4].

The above definitions for MC and MD are the accepted definitions in the field of molecular simulation. In terms of the general definition of Monte Carlo, Molecular Dynamics would still be considered a type of Monte Carlo simulation with regard to the fact that the choice of initial values for the MD simulation is essentially random. In addition, the method of extracting useful information from each simulation method is very similar. With Monte

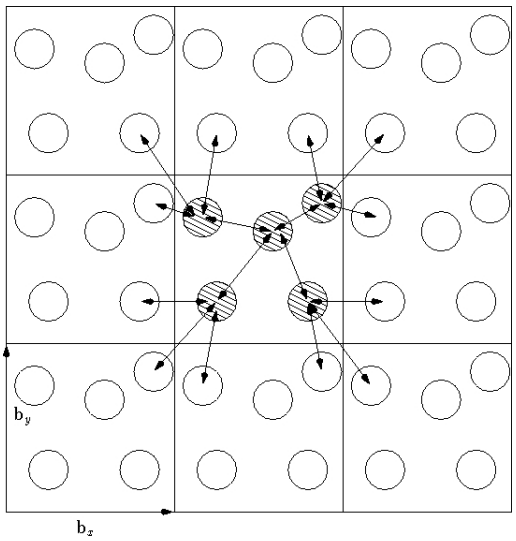

Figure 7: Periodic Boundary Conditions [85]

Carlo simulations one generally extracts useful information using averages over the sets of accepted confirmations which are non-time-dependent values. However with MD simulations one, again, is concerned with average values curves obtained through time-dependent autocorrelation functions. The distinction is the amount of deterministic calculation performed between the two methods. The simulationist's MC method relies almost completely on arguments based on energy and randomly generated positions while MD methods are based on Newton's Laws after the determination of the initial positions. Thus, as mentioned above, the most significant difference is how well time is defined. The calculations obtained from MD and MC simulations are equivalent under the assumption of ergodicity. Using ergodicity one assumes that if a MD simulation is run over a sufficiently long time period then most of the possible confirmations of the system have been explored and therefore the time average values obtained from MD simulations should be equivalent to the ensemble averages calculated via MC simulation.

Simplified polymeric models were simulated under constant density (NVT) or constant pressure (NPT) ensembles using the LAMMPS [69] molecular dynamics code available from Sandia National Labs. Simulations consisted of 80 ten-site (10 mer) chains and 5 single unattached 'penetrants' interacting

via Lennard-Jones (LJ) potentials and FENE potential bonds and integrated with a Verlet algorithm [84]. The chosen polymer model is similar to those explored in MD simulations by Kremer and Grest [45]. The temperature for all simulations and pressure for NPT simulations are maintained by algorithms inside LAMMPS based on methods developed by Nosé and Hoover [63]. Again since these algorithms are standard and taken without modification, the details are not discussed here. On a basic level, fluctuations of temperature or pressure are controlled through added energy terms in the system's Hamiltonian. The user defines the magnitude of these fluctuations through "friction factors."

A Lennard-Jones potential is an empirically derived potential given by equations 26-28 [87]. The simulations in this research used the LJ potential parameters σ and ϵ of argon.

$$U_{LJ}(r) = U_{LJ}^{R}(r) + U_{LJ}^{A}(r) \tag{26}$$

$$U_{LJ}^{R} = \begin{cases} 4\epsilon\left(\left(\frac{\sigma}{r}\right)^{12} - \left(\frac{\sigma}{r}\right)^{6}\right) + \epsilon & r \leq 2^{1/6}\sigma \\ U_{LJ}^{R} = 0 & r \geq 2^{1/6}\sigma \end{cases} \tag{27}$$

$$U_{LJ}^{A} = \begin{cases} 4\epsilon\left(\left(\frac{\sigma}{r}\right)^{12} - \left(\frac{\sigma}{r}\right)^{6}\right) + \zeta & R_c > r \geq 2^{1/6}\sigma \\ U_{LJ}^{A} = -\epsilon & r \leq 2^{1/6}\sigma \end{cases} \tag{28}$$

Since we are working in the numerical world, the potential must be truncated at some point R_c. The parameter ζ is added to the attractive part of the potential so that $U_{LJ}(R_c) = 0$ and we choose $R_c = 2.5\sigma$ for a full LJ simulation. We also consider separately a purely repulsive LJ potential which is clipped at its minimum. This is useful in that it greatly speeds up computation time but it does not affect our data when used for high temperature systems. That is, at high temperatures the contribution of attractive interatomic forces causes the system to have a higher density but does not alter the character of relaxation behavior as will be seen in later sections. In addition, the full force LJ simulations, which we call 'attractive', demonstrate a gas-liquid phase transition at high temperatures which is undesirable. The repulsive LJ simulations are equivalent to hard-sphere simulations in that they do not show this phase transition. Simulations are run on the order

of 10^7 to 10^8 time steps and correspond to nanosecond order experiments. These computations, however, can take up to several weeks to run.

The bonds are held together using finite extension non-linear elastic (FENE) [76] potentials.

$$U^{FENE}(r) = \begin{cases} -\frac{\kappa}{2} r_{bond}^2 \ln\left[1 - (r/r_{bond})^2\right], & for \;\; r < r_{bond} \\ \infty, & for \;\; r > r_{bond} \end{cases} \tag{29}$$

where $r_{bond} = 1.5$ and $\kappa = 30$.

Three different types of polymer models have been simulated. Freely jointed models have no constraining potentials on bond angles. In freely rotating models, the bonds angles are stiff and set to 120 degrees but are allowed to rotate freely. The bond angle potential is defined by the following function:

$$U_B(\theta) = K(\theta - \theta_o)^2 \tag{30}$$

where $\theta_o = 120$ degrees and K=0 for freely jointed systems and K=500 for freely rotating and 'torsion' systems. For 'torsion' models, torsion barrier potentials are added to the freely rotating model limiting the available dihedral angles. The potentials are defined as:

$$E = K_T(d + \cos(n\phi)) \tag{31}$$

where we define for our systems K=2.8, d=1, and n=3.

1.4 Diffusion and the Scalar Metric Revisited

Calculating diffusion constants for simulated polymers is relatively straightforward. In that sense, they are useful guide for determining the quality of simulation runs. This also makes them a convenient basis for finding a scalar metric. To calculate the diffusion coefficient of our polymer chains we first run a simulation of the chain which outputs position data. We determine the center of mass of each chain and then we calculate the mean squared

displacement (MSD) averaged over all of the chains in the system. The diffusion coefficient can be found using the Einstein relation [34]:

$$D = \lim_{t\to\infty} \frac{\left\langle |r(t) - r(0)|^2 \right\rangle}{6t} \tag{32}$$

where D is the diffusion coefficient and the statement in the angle brackets is the mean squared displacement. The method is altered for numerical data by simply plotting the MSD versus time and fitting a line of slope 6D to its long time region. An approximation for D is determined by performing the simulations long enough so that the linear region of the MSD plot covers more than a decade of time and by calculating D for many different runs of the same simulation.

We then use equation (33) to produce D^*, the dimensionless diffusion coefficient. The dimensionless version is used due to findings for scalar metric studies in hard-sphere simulation studies [36].

$$D^* = D\left(\frac{Nm}{(kTd^2)^{1/2}}\right) \tag{33}$$

where m is the mass of a bead, N is the length of the chain, k is Boltzmann's constant and d is the effective hard sphere diameter. The calculation of the effective diameter, however, is a potential source of difficulty. For simulations using only the repulsive part of the LJ potential we use the Barker Henderson [12] equation:

$$d^R = \int_0^\infty 1 - \exp\left(-\frac{U_{LJ}^R(r)}{T}\right) dr \tag{34}$$

Since this works for only for repulsive potentials it must be corrected for the full LJ potential (attractive) simulations. At this point we must now introduce the radial distribution function: $g(r)$. Traditionally $g(r)$ is obtainable through the Fourier transform of the structure factor obtained through scattering experiments [53]. The $g(r)$ is essentially the probability of finding another particle a given distance, r, from a chosen particle in the system. Thus if we choose a particle in the system, use the locations of the other

particles at all time-steps and repeat this for every particle in the system we can approximate the $g(r)$ for the system.

The radial distribution function for disordered systems is zero for $r < r_{particle}$ and then shows a sharp peak for $r > r_{particle}$. This location of this peak corresponds to the classical turning point of the interparticle collisions. Therefore it serves as a reliable measure of the effective hard sphere radius. Thus we use the following equation [18] to approximate d for the attractive LJ simulations:

$$d^A = d^R \left(\frac{r^A_{peak}}{r^R_{peak}} \right) \tag{35}$$

where the A and R stand for attractive and repulsive, respectively. Then packing fraction is calculated using:

$$\eta = \frac{\pi}{6} d^3 \rho \tag{36}$$

It is clear (figures 8 and 9) that packing fraction works very well as scalar metric for D^*. We see that D^* separates into constant density or constant pressures lines when plotted versus 1/T but collapses onto a single curve when plotted versus packing fraction, η.

1.5 Autocorrelation and Relaxation Functions

While the diffusion coefficient can tell us a lot about translational movements and relaxation in a material it does not tell us about configurational changes that are theorized to serve as the basis of macroscopic relaxation behavior. In addition, the diffusion coefficient is a single measure. One would like to obtain a level of detail of the relaxation as is available through modulus testing. This level of detail is obtained through the study of autocorrelation functions. An autocorrelation function measures how the configuration of the system at one initial time matches or "correlates" with the configuration at a later time. The actual application generally uses averages of the dot products of descriptive vectors. There are two autocorrelation functions of interest we will be looking at: the P_2 autocorrelation function and the dihedral autocorrelation function (DACF).

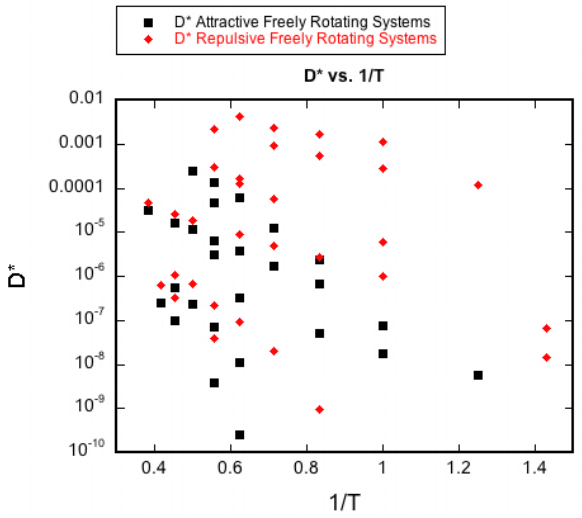

Figure 8: The square of D^* vs. 1/T. No apparent correlation

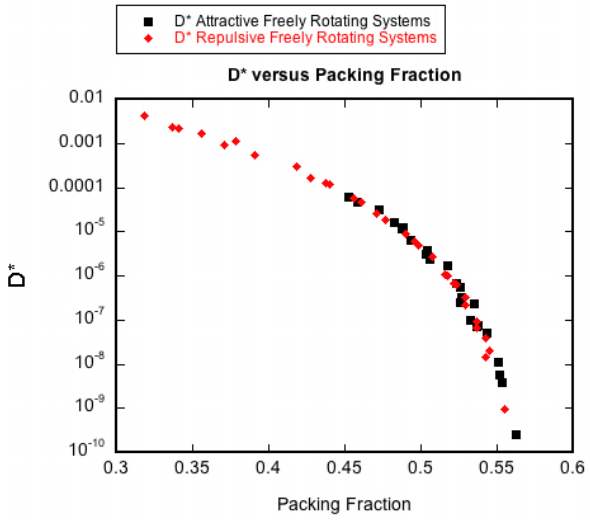

Figure 9: The square of D^* vs. η. Strong correlation

The P_2 autocorrelation function is determined from the simulation position data. It is calculated by equation (37) where $\overrightarrow{u\,(t)}$ is the vector drawn from the first mer in the chain to a later one (usually the last) and the angle brackets denote an average over all initial times and chains in the system. The P_2 function is believed to describe relaxation behavior of the polymer via the Fluctuation-Dissipation Theorem [46]. That is, the behavior of small fluctuations correspond to the reaction (i.e. dissipation) of the material to minute external perturbations. Therefore, the average P_2 relaxation of a system at equilibrium should be equivalent to the relaxation seen if we had applied a small deformation to the simulation cell or perturbed the chains themselves. This is an extremely important result as it allows to avoid difficulties in performing calculations for systems out of thermodynamic equilibrium.

The Fluctuation-Dissipation Theorem was formulated first for electric circuits by Nyquist [64] and then generalized by Callen [19]. The derivation of the theorem is outside the scope of this paper and can be found in the above articles. The important take-home message of the articles is that one is able to use fluctuation information from a system in equilibration to describe irreversible (dissipative) processes. The P_2 function is based on fluctuations in average chain orientation. Thus, by the Fluctuation-Dissipation Theorem, one would expect the P_2 autocorrelation function to relate most closely to dielectric relaxation results.

$$P_2\,(t) = \frac{3\langle \overrightarrow{u\,(0)} \cdot \overrightarrow{u\,(t)} \rangle - 1}{2} \tag{37}$$

Similar to the case of relaxation modulus, one can apply Fourier sine and cosine transforms to the P_2 function into to obtain data in frequency space. The real and imaginary parts are usually labeled $G\,(\omega)'$ and $G\,(\omega)''$ respectively. This notation reflects that of dielectric relaxation experiments.

There exist a number or other relaxation autocorrelation functions one can calculate which are often done as the simulated models become more and more complex. For the three systems of interest in this work, the dihedral angle autocorrelation function has also been calculated (38) [17] where ϕ is the dihedral angle. The DACF, like the P_2, is a calculated measure of relax-

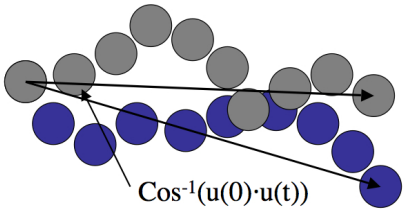

Figure 10: P2 Autocorrelation Angle

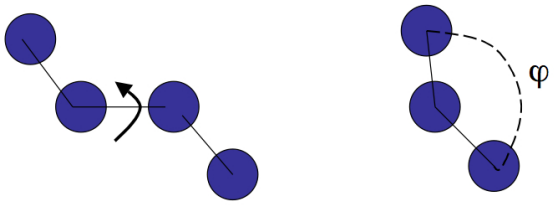

Figure 11: Dihedral Autocorrelation Angle

ation behavior. However, while the P_2 is primarily a measure of the rotational relaxation of most often the entire chain, the DACF measures the torsional relaxation between beads of the chain. That is, the two functions describe relaxation in two different axes which are perpendicular to each other this is illustrated in figures 10 and 11 and describe relaxation on two different length scales.

$$f_\phi(t) = \frac{\langle \cos\phi(0)\cos\phi(t)\rangle - \langle\cos\phi(0)\rangle^2}{\langle\cos\phi(0)^2\rangle - \langle\cos\phi(0)\rangle^2} \tag{38}$$

The angle brackets in equations (37) and (38) denote ensemble averages at each time t. An ensemble is the set of all possible states of a system. Clearly such a set is not practically obtainable through simulation. One makes the assumption of ergodicity, that is, such a set can be obtained by running the simulation for a sufficiently long period of time [8]. This assumption, however, begins to breakdown near the glass transition where the system falls out of equilibrium [51]. The averages are then calculated by averaging the set of curves obtained for every possible starting position. This is made more

clear by modifying equation (37) to reflect the actual method of calculation:

$$P_2(\Delta t) = \lim_{N\to\infty} \frac{\sum_{i=1}^{N} \vec{u}(t_i) \cdot \vec{u}(t_i + \Delta t)}{N} \tag{39}$$

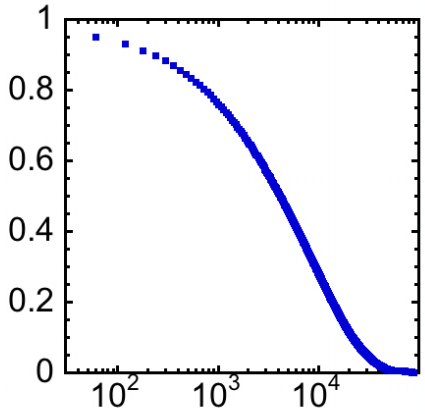

Figure 12: P_2 autocorrelation function for a repulsive FR system of LJ temperature 1.6 and density 1.06

2 Fitting Autocorrelation Functions

The plots of these autocorrelation functions tend to be relatively featureless non-exponential decays (figure (12)). This lack of landmarks in the plot not only makes the choice of fitting function difficult but also the choice of inversion algorithm. It also poses difficulty because the source of the non-exponentiality of the decay is a point of contention. There are two viewpoints of the basis of non-exponential decay: homogeneous and heterogeneous. The microscopic level is often qualitatively (but unrealistically) described as particles moving through a frictional medium such as the picture obtained from Langevin's treatment of brownian motion [34]. A homogenous explanation claims that each molecule in the system shows the same decay behavior and this behavior happens to be non-exponential, that is, the friction imparted by the medium does so as to produce non-exponential decay behavior for each molecule. The heterogeneous picture is that each molecule at a particular moment in time and position in space only demonstrates single exponential decay and it is variations and movements, in time and space, of different frictional regions that as an ensemble average produces non-exponential decay of the system as a whole. A more detailed exploration of this issue can be found in an excellent article by Ediger [27]. These two physical explanations, are contradictory in terms of the underlying physics and this fact needs to be addressed when considering which model to use in one's fit [37].

2.1 Spectral Method

The model assumption is the following Fredholm Integral Equation (IFK) of the 1st kind:

$$P_2(t) = \int_{-\infty}^{\infty} G(\tau)\, e^{-t/\tau} dln\tau \tag{40}$$

The use of this equation implies that the relaxation process is the superposition of many single exponential decays, that is, heterogeneous. Given the flexibility and number of fit parameters, it is not very difficult to obtain a very good fit of the data. Unfortunately, the kernel of the IFK, $e^{-t/\tau}$, is not orthogonal [40]. That is, for the inner product defined by the integral over the entire real line the set of functions $e^{-t/\tau} \quad \tau \in \Re$ is not orthogonal. Indeed, it may be very difficult to produce a subset of this set which is

orthogonal. Thus, the inversion of this IFK is significantly ill-posed. Therefore, the obtained distributions are non-unique and it becomes necessary to regularize the solution is some fashion. Constraining the non-negativity of $G(\tau)$ is an obvious and powerful way to eliminate oscillating solutions. A few regularization methods are discussed in the next section. A broader exploration of spectral methods was performed by Istratov [40]

The most common method for solving for distributions of relaxation times (DRT's) is Tikhonov Regularization. Tikhonov Regularization is a variation to standard Least Squares methods. Using the notation of the standard inverse problem: $Gm = d$ where G is the operator, m is the model and d is the data, instead of minimizing $\|Gm - d\|_2$ we instead minimize $\|Gm - d\|_2 + \alpha^2\|Lm\|_2$ where α is the regularization parameter and L is the regularizing operator (often the identity or a derivative operator). The integral equation is reduced to the standard matrix-vector inverse problem either through simple quadrature or a series of representing function. These methods are described in detail in standard inverse problems texts [11].

A commonly used program in producing Tikhonov regularized solutions is CONTIN, developed by Provencher [71]. Karatosos and Adolf [43, 42] and others [10, 6, 3] have utilized CONTIN to obtain DRT's of relaxation functions. CONTIN determines the regularization parameter by invoking the Principle of Parsimony, that is, by increasing the degree of regularization until the point that the curve fit begins to break down. A more accessible constrained Tikhonov regularization MATLAB script was developed by Berglund [16] and several different methods for determining the regularizing parameter for a given problem exist [11].

However, it should be noted that the gain in stability in using Tikhonov regularization is matched by a loss in informational resolution. Therefore, one must be careful of the confidence one has in the obtained model, especially with inversions where a priori knowledge of the expected model is lacking.

2.2 Multi-exponential Model

Another heterogeneous model is a sum of decaying exponentials or multi-exponential model. The difference between the multi-exponential and spec-

tral models is that the spectral model is a linear inverse problem where one seeks a continuous underlying distribution while the multi-exponential model is a nonlinear problem which conveys similar information as the spectral model but assumes the spectra to consist of a series of delta peaks. The aforementioned review by Istratov includes several methods for multi-exponential models not covered in this article. This paper deals with only the most pertinent methods.

The Levenberg-Marquardt (LM) algorithm is a robust variant of Gauss-Newton (GN) optimization (based on Newton's root solving algorithm). It is discussed in detail in the original papers [49, 54] and in the text [11]. It differs from the GN method by the inclusion of an additional parameter to ensure convergence. A notable difficulty in the method arises when there exists several local minima in the plot of the residual in parameter space. It becomes difficult to identify the global minimum of the problem. Unfortunately, this is exactly the case in fitting a sum of exponentials. One can work around this problem by utilizing several different but reasonable initial guesses. This is referred to as the Multi-Start Method [11]. Additionally, the locations or relative positions of the delta peaks can be user-defined to remove degrees of freedom but without any theoretical reasoning this choice will be arbitrary and limit the usefulness of the results.

2.3 The KWW and CD functions

Spectral and multi-exponential methods indeed provide very good fits of the data, however, they are incapable of providing any clarity or insight into the basis of the physical relaxation phenomena. If the intention of the research is be able to relate the relaxation behavior to physical descriptors such as a scalar metric then unique physically significant model parameters are necessary. The difficulty with spectral methods is that in order to limit the instability of the algorithm with regard to error one must lose information through regularization. Additionally, it is arguable whether or not the transformation into decay constant space provides any clarity of physics because the spectrum is more difficult to describe and fit than the relaxation function itself. The problems associated with multi-exponential fitting are non-uniqueness and limits in resolving close peaks. Also, there is a lack of clear theoretical justification for one distribution of peaks versus another.

Therefore the next functions of interest are chosen for their importance in experimental research and their relatively small number of degrees of freedom. The direction of the research is very much into finding or refuting the physical significance of the parameters in these functional forms.

The P_2 function is very often fit in time space using the Kohlrausch-Williams-Watts (KWW) or stretched exponential function:

$$P_2(t) = e^{-(t/\tau_{KWW})^{\beta}} \tag{41}$$

which was first applied to capacitor discharge by Kohlrausch [44] and later rediscovered and applied to dielectric relaxation by Williams and Watts [88]. The KWW function, however, has its own difficulties. Generally, it does not fit the early and late regions of the decay very well and the β changes quite substantially depending on how much of these early and late regions one attempts to fit [14] in addition to the amount of error present. In past literature the choice of the KWW region has been mostly arbitrary. However, the benefit of using a KWW fit is that it is very stable once a consistent methodology for the fit region is developed. The β, which when written as $n = 1 - \beta$ is the degree of non-exponentiality, is a very attractive candidate as a system specific descriptor of relaxation behavior. Additionally, one can make either an argument for a homogeneous or heterogeneous picture of the decay physics as the stretched exponential has an associated spectrum for each beta. As one can see in figure 13, the spectrum broadens with decreasing beta [50].

In frequency space relaxation functions are not generally fit with a Fourier or Laplace transform of the KWW function but instead with the Cole-Davidson [24] (CD) function:

$$\frac{\epsilon(\omega)^* - \epsilon_\infty}{\epsilon_0 - \epsilon_\infty} = \epsilon'_N(\omega) - \imath\epsilon''_N(\omega) = \left(\frac{1}{1 + \imath\omega\tau_{CD}}\right)^{\beta_{CD}} \tag{42}$$

where the subscript N denotes that the storage and loss parts of the function are normalized and the zero and infinity denote low and high frequency limits respectively. Unless β=1, $\tau_{KWW} \neq \tau_{CD}$ and $\beta_{KWW} \neq \beta_{CD}$. The KWW and CD functions appear almost indistinguishable in time space, however, their

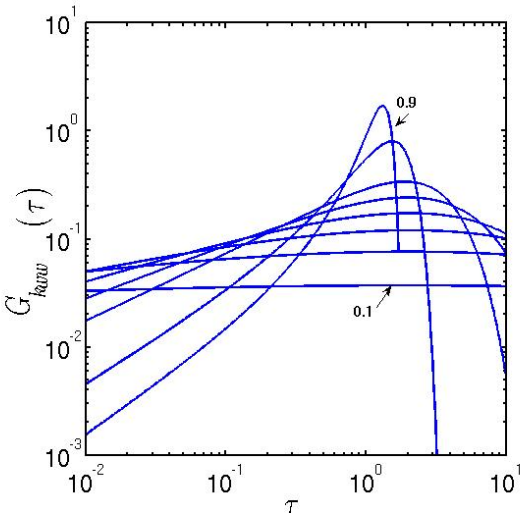

Figure 13: τ spectrum of KWW function for different βs [50]

spectra are very different (figure 14) until β approaches a value of 1 (figure 15). A more in-depth evaluation and comparison of the KWW and CD functions was performed by Lindsey and Patterson [50].

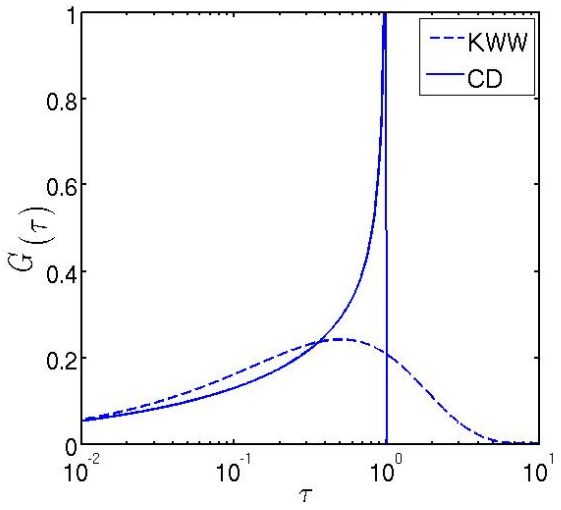

Figure 14: Spectrum of KWW and CD functions: β_{KWW}=0.5, β_{CD}=0.37, τ_{KWW}=0.25, τ_{CD}=1.0 [50]

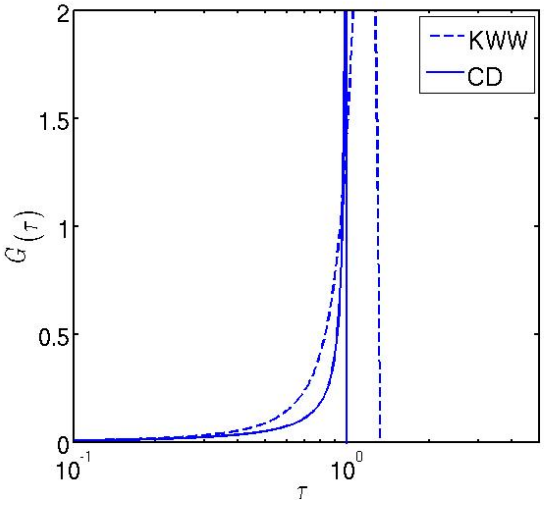

Figure 15: Spectrum of KWW and CD functions: β_{KWW}=0.95, β_{CD}=0.95, τ_{KWW}=1.0, τ_{CD}=1.0. Note how both spectra are starting to resemble delta functions.

3 Relevant Theoretical Models and Spin Glasses

There have been a number of attempts to formulate theoretical basis for the relaxation behavior seen in viscoelastic materials, unfortunately, no such theory has yet shown itself to be the definitive theory of relaxation and/or the glass transition. I cannot cover all such theories since they are far too numerous but I will provide an outline of the most pertinent. A detailed explanation of these theories is outside the scope of this paper but can be found in the accompanying references. I will stress only what is important for this research. In addition, in this section I provide some information about spin glasses with which much research has been done into the possible basis of glassy behavior.

3.1 Rouse Model

Recalling the derivation of the equations of Time-Temperature Superposition in section 1.1.4 the reader may remember that results from the Rouse Model were utilized. The Rouse Model was perhaps the earliest theory of polymer dynamics [75]. A polymer chain in the Rouse Model is represented by a number of beads (N) connected by springs with root mean square (RMS) length b. The beads only interact through the springs and each bead's behavior is influenced by its own individual friction coefficient ζ. Using the Einstein relation:

$$D = \frac{kT}{\zeta} \tag{43}$$

The Rouse Model predicts the diffusion coefficient for the chain to be [76]:

$$D_R = \frac{kT}{N\zeta} \tag{44}$$

and thus one can obtain a characteristic "Rouse time" where the chain diffuses a distance comparable to its size.

$$\tau_R \approx \frac{R^2}{D_R} \tag{45}$$

The size of the chain is generally related to the number of monomers by a power law.

$$R \approx bN^{\nu} \tag{46}$$

where $1/\nu$ is the fractal dimension of the polymer.

Unfortunately this prediction for the diffusion coefficient is not consistent with experimental results [26] as the diffusion coefficient for dilute polymers is instead found to be proportional to the reciprocal of the square root of N. However, from the Rouse Model one can derive a prediction of the end-to-end autocorrelation function (that is, P_2) [26].

$$P_2(t) = Nb^2 \sum_{p=1,3,5\ldots} \frac{8}{p^2\pi^2} \exp -\frac{p^2}{2\tau_R} t \tag{47}$$

As successive squares of small odd integers differ by more or less than factors of two it is clear from the discussion presented in [40] that such a model may be impossible to confirm. This is because the resolution for spectral and multi-exponential methods is not, generally, fine enough to separate peaks differing by less than a factor of two. The results of the application of this model to our simulation results can be found in section 5.2.

3.2 Mode Coupling Theory

While the Rouse Model primarily deals with dilute polymer dynamics, Mode-Coupling Theory (MCT) attempts to describe the onset of the glass transition and was first developed by Leutheusser [48] and Bentzelius et al. [13]. The idea behind MCT is that the fluctuation of a dynamic variable decays through hydrodynamic modes [34]. That is, there exists a feedback mechanism through which these fluctuations in the structure slow down and cannot relax [47]. These relaxation modes are generally described by relaxation spectra (see section 2.1). The glass transition is explained in the theory by particle "caging" [31]. Particle caging is the idea that as a liquid becomes more and more dense the neighboring particles form a sort of cage around each other and that a particle must then do more and more work to escape this cage.

An important prediction of MCT is that the longest relaxation time scales as a power law [47]:

$$\tau_\alpha \propto (T - T_C)^{-\gamma} \tag{48}$$

where T_C is the critical temperature for the onset of the glass transition. The immediate result of this prediction is that near the glass transition one would expect viscosity to scale by this same power law as opposed to the Vogel-Fulcher equation given earlier (equation (25)). It is also important to note that $T_C \neq T_0$. Unfortunately it has been found that relaxation/viscosity data is only described by a power law over a limited range and the Vogel-Fulcher seems more appropriate. Götze and Sjögren [31] claim that this does not necessarily imply a violation of MCT but that T_C is not the glass transition temperature but an important intermediate temperature between the glass transition temperature and a temperature where the relaxation behavior is approximately Arrhenius.

It has been found that some relaxation modes slow down at the glass transition (α relaxation modes) and some do not (β relaxation modes) [41]. Consequently, it is then these α relaxation processes that are of particular interest of researchers. In addition, these modes dictate material behavior on intermediate to long timescales while β processes deal with fast decaying atomic and quantum level phenomena. More detailed treatments of MCT can be found in [72].

3.3 Coupling Model

The Coupling Model (CM), introduced over 30 years ago [56], has been primarily the work of K.L. Ngai. The Coupling Model attempts to be a general theory of relaxation. The idea behind CM [60] is the picture of a cooperative system of identical relaxing species (such as ions in a viscous conductor or entangled polymer chains). At short time the particles can be considered to be non-interacting at short time and thus the relaxation rate is constant:

$$W(t) = W_0 \tag{49}$$

After some critical time, t_C, the molecules interact more strongly and thus the relaxation becomes slowed down. The relaxation rate is then:

$$W(t) = W_0 (t/t_C)^{-n} \tag{50}$$

where,$0 \leq n \leq 1$, is the "coupling parameter" which is a measure of the degree of interaction and non-exponentiality. If one then solves for the relaxation function, using $W_0 = 1/\tau_0$ one finds:

$$\phi(t) = \exp\left[-\int_0^t W(s)\, ds\right] = \begin{cases} \exp\left[-t/\tau_0\right], & t < t_C \\ \exp\left[-\left(t/\tau^*\right)^{1-n}\right], & t > t_C \end{cases} \tag{51}$$

where,

$$\tau^* = \left[(1-n)\,\omega_C^n \tau_0\right]^{1/(1-n)} \tag{52}$$

So we see that CM predicts the short time behavior to be essentially Debye. This is a very important part of CM. As one can see in equation (50), if this assumption were not made the relaxation rate would diverge in the limit $t \to 0$.

In [60], Ngai et al. argue that a heterogeneous picture of relaxation, such as given through spectra or distributions of relaxation times (DRT), is incompatible with the Coupling Model. They list a number of reasons for this. For one, the relationship between τ_0 and τ^* differs depending on whether the KWW function was constructed from a Coupling Model or a DRT approach. Their argument is that the interactions affect the relaxation in a way as to make it non-exponential and not that is arises from the superposition of single exponential Debye processes. A more in depth discussion is contained in the article mentioned above. The main limitation of CM seems to be that it does not provide a detailed explanation of molecular level relaxation processes and how these exactly contribute to overall macroscopic behavior. Additional information about the Coupling Model can be found in the already cited articles and in [58, 83]. Also, Philips has published a detailed review of stretched exponential relaxation behavior [67].

3.4 Spin Glasses

A spin glass is a material that exhibits high magnetic frustration, that is, it demonstrates an inability to remain in its ground state. A spin glass's behavior with respect to magnetization is very similar the behavior of viscoelastic materials with respect to mechanical deformation. Below the material's spin glass transition temperature, when an applied magnetic field is removed,

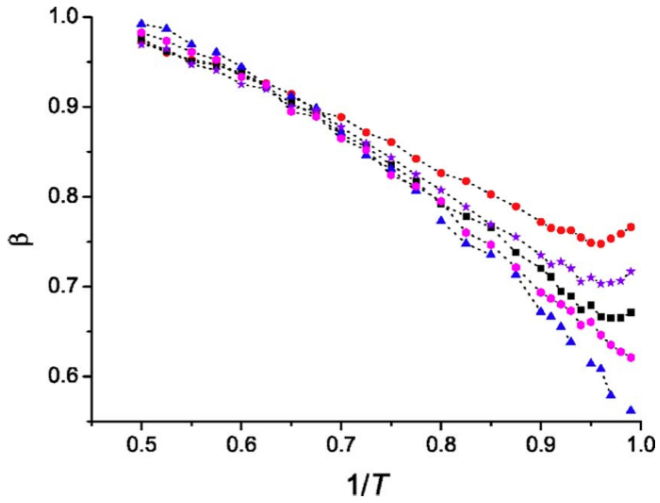

Figure 16: Changing β for 3-dimensional Potts model. q = number of fractional spins available. q = 3 circles, red, q = 4 stars, violet, q = 5 squares, black, q = 6 hexagons, magenta, and q = 8 triangles, blue [33].

the magnetization decays non-exponentially. As a result, spin glass models are useful in the study of viscoelastic behavior [5]. Spin glasses are often modeled by an Ising spin model or the more general Potts model. Such models are constructed from large arrays of interacting spins. In such models correlation and autocorrelations are important in defining relaxation functions for the systems. Researchers have found that one-dimensional Ising [52] and 3-dimensional Potts [33] models exhibit physical glass behavior such as stretched exponential decay and Vogel-Fulcher scaling of decay times. The research on the 3-dimensional Potts model utilized KWW functional fits on the function P(t) which was the fraction of spin sites that had not changed spin. Halpern found actually found the parameter β for these functions to vary with temperature which implies that TTS does not apply to these model systems.

4 Research Context: Physical Aging and Material Clocks

At this point it becomes necessary to draw out the larger context for the following research. It is probably not exactly clear to the reader how these relaxation function relate to the mechanical moduli. The relationship between relaxation functions and dielectric data was made clear in section 1.5 when discussing the Fluctuation Dissipation Theorem. The relaxation spectra of mechanical and dielectric data do differ [1], however, they appear very similar when one narrows their view on the α relaxation region which was introduced in the section on Mode Coupling Theory [22].

One important application of this research is in the field of physical or structural aging of polymers. Physical aging is the variation of physical variables of a material as it approaches equilibrium after a perturbation [51]. If we recall the discussion of viscoelastic behavior in the introductory chapters, we know that physical relaxation, as occurs in a material approaching equilibration, can occur over timescales beyond what is practical experimentally (often much longer than the expected lifetime of the typical experimentalist). For this reason, computer simulation, among other methods, is used to provide the information with which one could predict long-term performance of these materials.

Additionally, the picture of viscoelastic mechanical behavior in section 1.1.1 is a greatly simplified view. In reality, engineering objects using viscoelastic materials is very difficult because one often operates in a range where the response in nonlinear and the glassy nature of the material means that one is dealing with a substance not in equilibrium. As a result, there is a great deal of research into developing what are called nonlinear constitutive models that can predict these more complicated material responses in addition to the long-term behavior [55]. Such models often make use of "material clocks." A material clock is a reduced material time, depending on the current state and history of the material, that dictates the relaxation behavior and may differ greatly from laboratory time. An overview of constitutive models and material clocks can be found in the article by McKenna [55]. The clocks in the models reviewed by McKenna either depend on stress or free volume. A recent model developed D.B. Adolf et al., instead, looks to potential energy

to describe the material time [2]. If such a constitutive model shows itself to adapt well to predicting viscoelastic behavior, it could then be used in Finite Element codes to be used by engineers.

The research presented in this paper fits into a proposed constitutive model by providing detailed information about how the relaxation of a material changes with respect to state variables. This information is hoped to fit into a theoretical framework of the glass transition such as Mode Coupling Theory so that one is better able to predict the behavior. For example, if one is working within the context of Mode Coupling Theory one would attempt to fit the various relaxation parameters with power laws:

$$\tau = (T - T_C)^{\gamma} \tag{53}$$

where one could of course substitute some scalar metric in place of temperature, T. The details of such analysis is outside the scope of this paper. The general idea is presented in order to help answer any questions of why such research is being performed.

5 Methods and Results

5.1 Spectral

Very quickly in the search for a procedure for analyzing our autocorrelation functions it became clear that the spectral methods were not practical. The first limitation of the method is the loss of information as a result of the need to regularize. Because of this, it is difficult to believe in the reality of the obtained spectrum. Since one of our intentions in the research is the evaluation of Time-Temperature Superposition, this level of uncertainty is undesirable. One of the main stipulations of TTS is that all relaxation times of a system should shift the same with a change in temperature. In other words, the distribution does not change from one temperature to another. Thus we are stuck with the problem of the subjectively deciding what kind of variation in spectrum would be significant enough to signal that TTS has been violated.

In addition, the obtained distribution is very much dependent on the method of regularization. One could employ the parsimony principle, as used in the CONTIN program mentioned earlier, but then one is left trying to make judgements about significant variations in the distribution for a set of distributions that is not believed to truly reflect the reality of the physical phenomena.

The third limitation of the method is that such a procedure does not very much simplify our view of the data. The obtained spectrum is more complicated and more difficult or impossible to describe by a single function than the original relaxation function. What is, instead, of practical interest is a method resulting in a manageable number of physically relevant parameters.

5.2 Multi-exponential Model

The situation for a multi-exponential approach is slightly better. One can use the predictions of the Rouse model (equation (47)) to attempt to regularize the problem. In order to evaluate this method the following fit was performed:

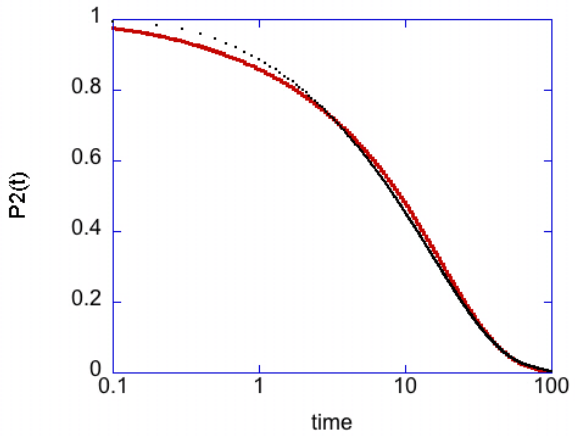

Figure 17: Eleven Term Multi-Exponential Fit: Low Packing Fraction

$$P_2(t) = A\left[\exp -t/\tau + 1/9 \exp -9t/\tau + 1/25 \exp -25t/\tau + \ldots\right] \qquad (54)$$

The results of an eleven term fit for two systems on opposite ends of the simulation range, in terms of packing fraction, are show in figures 17 and 18.

This procedure clearly leaves a lot to be desired in terms of fitting the data. Even with a relatively large number of terms the P_2 function is not adequately described. There are many reasons for the failure of this methodology. First, the very use of this functional form assumes Time-Temperature Superposition to hold. The fit is seen to transition from underestimating the shorter time region at low packing fractions to overshooting it at high packing fractions. This systematic failure of the fitting procedure seems to suggest that TTS does not hold for our systems. Second, the coefficients of our exponential series decrease as n^{-2}. Thus if our relaxation curve is not well described by two to three exponentials then it is unlikely that we will obtain a reasonably good fit with a Rouse model at all.

Without the ability to use the Rouse model as a guide the situation is very similar to that of spectral methods. Clearly we will need more than two degrees of freedom in describing this function with a sum of exponentials barring some new theoretical motivation as to the specific form of the series.

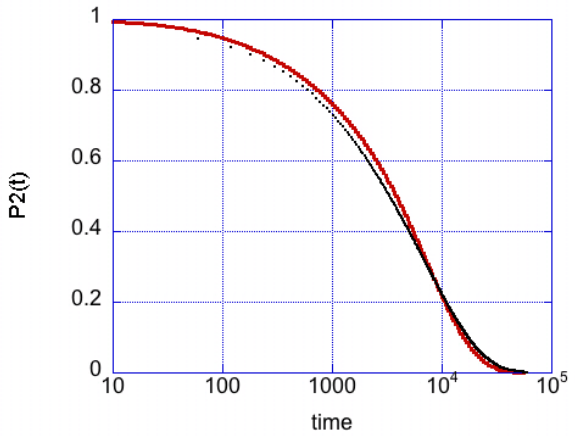

Figure 18: Eleven Term Multi-Exponential Fit: High Packing Fraction

If one uses very few parameters in constructing a fit of the data the assumption of Time-Temperature Superposition is often necessary. On the other hand if one wants to fit the function as a way to explore whether or not TTS should be assumed then one tends to get bogged down in a large number of degrees of freedom. In the latter case, the ill-posedness of the problem makes it very difficult to then reduce the number of parameters to something more reasonable and again it is hard to judge what kind of variation in any of these parameters to be significant.

5.3 The KWW Model

The KWW stretched exponential function is a very attractive choice in light of the above problems. The advantage of the KWW function is that it works very well for a large variety of data. The main source of difficulty in the KWW fit is the determination of the region of fitting. The P2 function generally exhibits non-stretched (non-KWW) behavior at very short and very long times. At long time, the function behaves similar to a single exponential until the function becomes noise limited at approximately $P_2(t) = 0.05$ or later depending on the quality of the simulation run. It is unclear, however, exactly where the noise becomes dominant and it is possible that the func-

tion actually becomes non-exponential in the region before becoming noise limited.

5.3.1 The Ballistic Region

At short time the P2 function displays 'ballistic' behavior. The behavior in this regions is not adequately described by a single exponential (figure (19)). It is described better when a stretched exponential fit is used up but this fit often fails as well and unnecessarily influences other regions of the fit making it more difficult to correctly nail down β. The idea behind the term 'ballistic' is that it is assumed that at short times the chains have not felt the potentials of their neighbors and thus are moving at constant angular velocities. Thus, one assumes this behavior is approximately described by $P_2(t) = \frac{3}{2}\cos t - \frac{1}{2}$ then to a rough approximation the short time behavior of the plot of $\ln - \ln P2$ is close to linear with a slope of two. Fitting the cosine to the earlier region appears to be more accurate for some systems and impossible for others. This is probably due to the discrete sampling of the P_2 function. As the ballistic region is not expected to shift with state point one ends up losing the necessary data to resolve this region as one simulates systems that relax more and more slowly. Getting the LM algorithm to converge for this method is also difficult. An additional concern is whether the numerical precision in the algorithm becomes a significant factor at such early times where thousands of numbers very close to one are averaged.

However, the ballistic region does not seem to be of much interest experimentally. What will be found in section 5.3.3 is that this region can be fit reasonably well by extending the obtained stretched exponential function to short times. Additionally, as we will see when the Cole-Davidson function is explored, a very accurate fit of this region does not significantly impact the representation of the relaxation function in frequency space as this region gets lost in the high frequency noise. Therefore, we will focus instead on the more important intermediate to long-time regions of the P_2 autocorrelation function.

Regardless of which model: KWW, spectral or multi-exponential, is used it is not very difficult to produce a very good fit of the data. Unfortunately, these fit often have some degree of non-uniqueness and the minimum of the

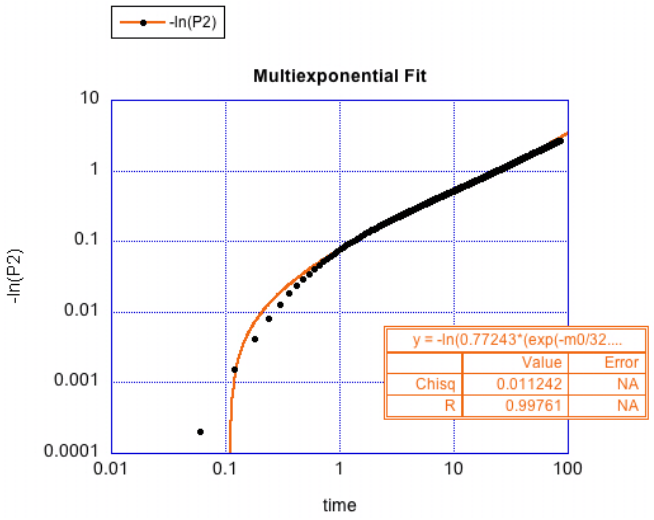

Figure 19: Multi-exponential Fit of "Ballistic" Region

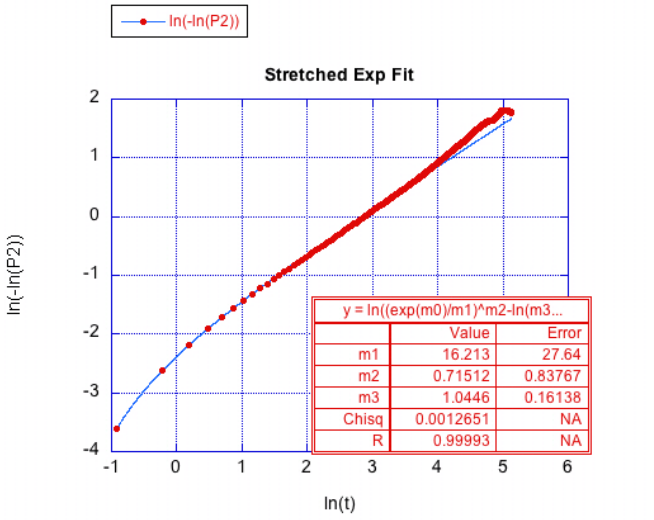

Figure 20: Stretched Exponential Fit of "Ballistic" Region

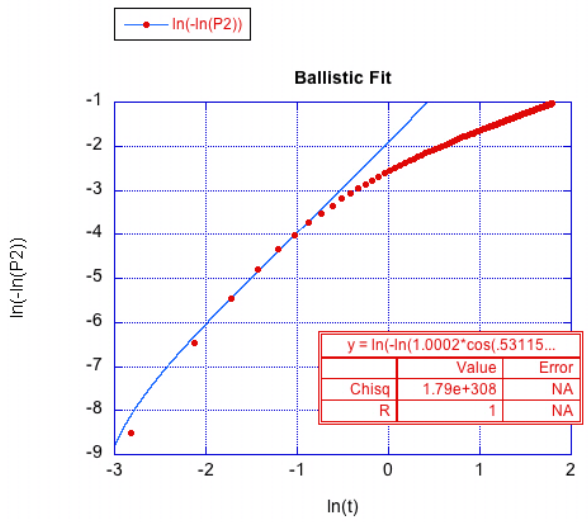

Figure 21: Cosine fit of "Ballistic" Region

residuals in parameter space tend to be shallow or contain multiple local minimums. Therefore one often obtains large uncertainties with regard to the exact values of the parameters. It then becomes difficult to decide which P2 parameters are changing and which staying the same in group of simulations at different state points.

5.3.2 Time-Temperature Superposition Revisited

The principle of Time-temperature superposition would suggest that the P2 functions of these different simulations should overlay given a correct scaling of the axes and indeed they appear to overlay to some extent depending on when one considers the 'ballistic' region to end and where the single exponential region begins. However, given how relatively featureless the P2 functions are, it is difficult to know what kind of variances between different relaxation functions are truly significant. Such an overlay, shifting the curves such that all the curves line up at $P_2(t) = 0.5$, is shown in figure (22). If the raw data overlays without difficulty one expects the functional fits to have parameters, which given the same scaling, are the same. For example, one would expect the β for the KWW fit to remain constant or the relative positions of the multi-exponential decay constants and the magnitudes to remain the

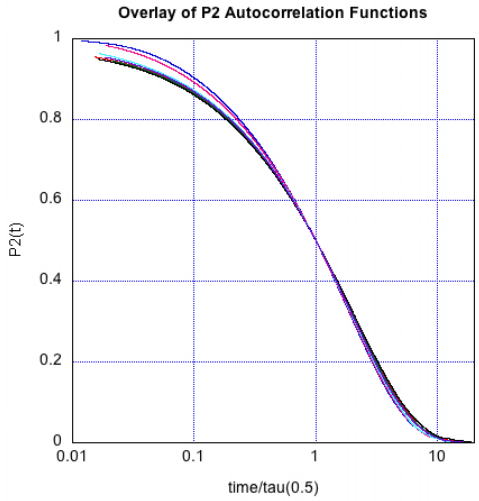

Figure 22: Overlay plot of P2 decays for several different state points

same (see discussion in section 1.1.4). Unfortunately, depending on which region of the function one fits with a stretched exponential, the extent of the ballistic region and the error present, the β can change to such an extent as to make an attempt to correlate it with packing fraction, or another scalar metric, impossible. Clearly a consistent method of determining the region of the fit is necessary to determine whether or not the parameter is changing.

5.3.3 Method for Fitting the KWW function to P_2 Relaxation Functions

We have developed such a method. The "stretched" region is found through plotting what has been termed the Lindsey-Patterson (LP) form:

$$\ln\left(-\ln P_2\left(t\right)\right) \tag{55}$$

against the Modified Lindsey Patterson (MLP) form:

$$\ln\left(-\frac{d\ln P_2\left(t\right)}{d\ln t}\right) \tag{56}$$

and finding where the slope is one. Given the assumption that P_2 has KWW behavior, one is plotting

$$\beta\ln t-\beta\ln\tau+\ln\beta \tag{57}$$

versus

$$\ln\left[\left(\frac{t}{\tau}\right)^{\beta}-\ln A\right] \tag{58}$$

Then, in the region where $\left(\frac{t}{\tau}\right)^{\beta}\gg\ln A$ the second term reduces to

$$\beta\ln t-\beta\ln\tau \tag{59}$$

and thus one expects a slope of one in the stretched exponential region given that our approximation is valid. Since A is almost always very near to one, a region where this approximation is valid has been found for every obtained P_2 function. One then plots the LP form, the modified LP form and the original P_2 versus $\ln t$ over this reduced domain and find the parameters β, τ_{KWW}, and possibly A for each one using a Levenberg-Marquardt algorithm. However, the numerical derivative greatly magnifies the error present and may make it difficult to find a slope one region. As a result, much of the data accumulated by previous students was not of high enough precision to be usable and a great deal of work was required to reduce the numerical error present in the data.

The graph in figure 23 demonstrates how one finds the stretched exponential region using this method. The validity of the approximation in equation (59) is confirmed if a slope one region is found for the system. As a result of this assumption the determined stretched exponential region can be found to be very small. Fortunately, the KWW function constructed by the obtained parameters seem to adequately describe a much larger region. The constant, A, is often reintroduced into the fit of P_2 on the restricted time domain in order to confirm that the region conforms to the approximation. Interestingly enough, when this parameter, A, is used in the fitting P_2 versus time the

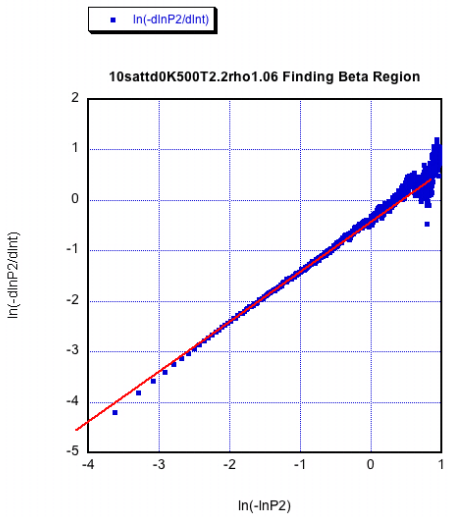

Figure 23: $\ln\left(-\frac{d\ln P_2(t)}{d\ln t}\right)$ versus $\ln\left(-\ln P_2\left(t\right)\right)$

obtained beta is very close to the β found when fitting the modified Lindsey Patterson form but when A is assumed to be one the obtained β is much closer to the value obtained from fitting the regular Lindsey Patterson form. Solving for β and τ_{kww} for several different packing fractions (figure 5.3.3) leads to strong argument for a changing β which would appear to violate TTS. According to some, this would imply that system is near the glass-transition [68]. However, given that the correlation between β and packing fractions holds for very low packing fractions, this cannot be the case.

What we see in figures 5.3.3 and 26 is that the relaxation behavior is very close to Debye-like at low packing fractions and β decreases with increasing packing fraction. According to the Coupling Model we are seeing this as a result of increased interaction between the chains. It is interesting that the curve for freely jointed systems has begun to level off at a nonzero value of β. Thus, the simulation material is rheologically simple (i.e. TTS holds) only at higher packing fractions. The curve for the freely rotating systems may just be beginning to level off but one cannot know for sure until our computational capacity improves.

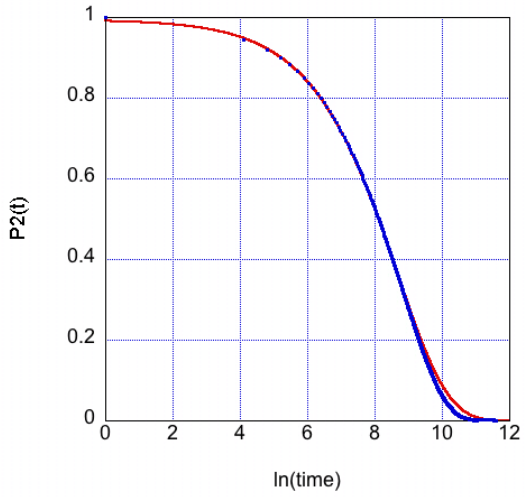

Figure 24: Stretched Exponential Fit

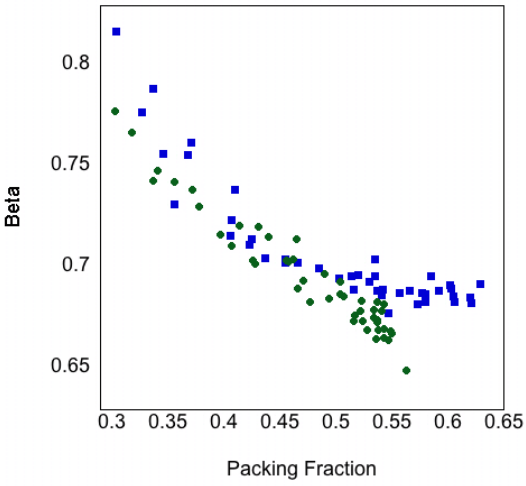

Figure 25: Changing Beta for Freely Rotating (Circles) and Freely Jointed (Squares) Systems

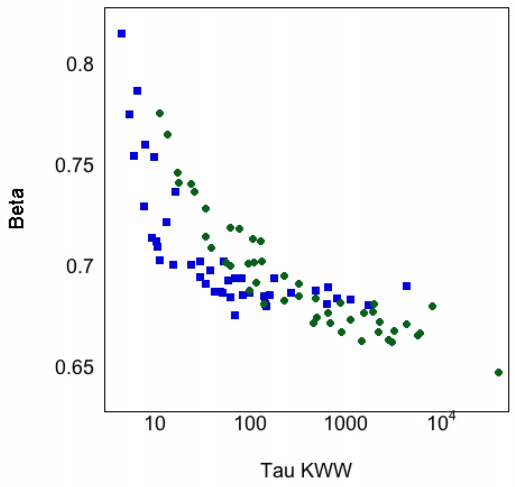

Figure 26: Changing Beta for Freely Rotating (Circles) and Freely Jointed (Squares) Systems

A non-constant β is not without precedent in the literature. It is very often seen in the experimental work of Ngai and his colleagues [59, 57, 66] and we saw earlier that it occurs in spin-glass models of viscoelastic behavior. Since packing fraction is generally difficult to obtain experimentally, most researchers plot β versus τ_{KWW}. In order for us to better connect our results with experiment, it is useful to plot β versus τ_{KWW} (figure 26).

After fitting the stretched region it is relatively simple procedure to fit the single exponential "tail" region. This region, however, generally contains much more error as a result of the method of calculation (see section 1.5). One approach is to roughly determine the domain of the single-exponential tail by performing a log transformation of the data and finding the long-time linear region then performing a weighted LM fit of the untransformed data on this restricted domain. One expects the residuals of this fit to vary systematically in the region better described by another function (such as the stretched exponential) and this is indeed found to be the case (figure 27). Repeating this procedure for several iterations one ends up with a very reasonable fit of the data (figure 28).

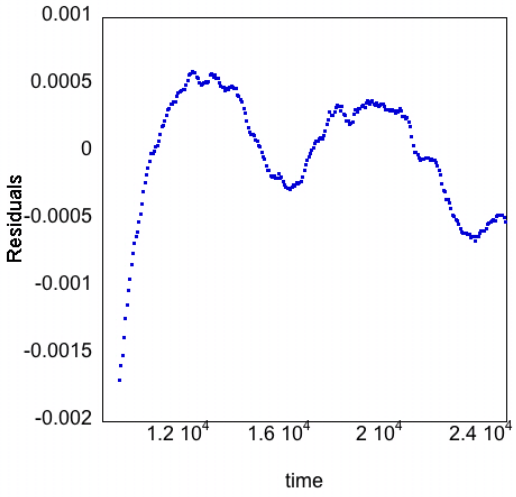

Figure 27: Residuals Obtained Fitting Tail Region with Single Exponential

From the results of this fitting procedure across a large number of systems one can see that τ_{tail} scales with τ_{KWW} (figure 29). Additionally, the constant, B, is seen to correlate with packing fraction in the same way as β (figure 30), however, with a great deal of scatter.

5.3.4 The KWW Model in Frequency Space

These methodologies have allowed us to have a little more confidence in our obtained values. The restricted domains found for both the stretched exponential and single-exponential regions are often relatively small. However, the piecewise combination of these two functions appears to describe the entire curve very well and additionally the two curves match very closely in the cross-over region. We can evaluate this description of the $P2$ function more quantitatively by performing the following transform:

$$P_2(\omega) = \int_0^\infty -\frac{dP_2}{dt} e^{-\imath\omega t} dt \tag{60}$$

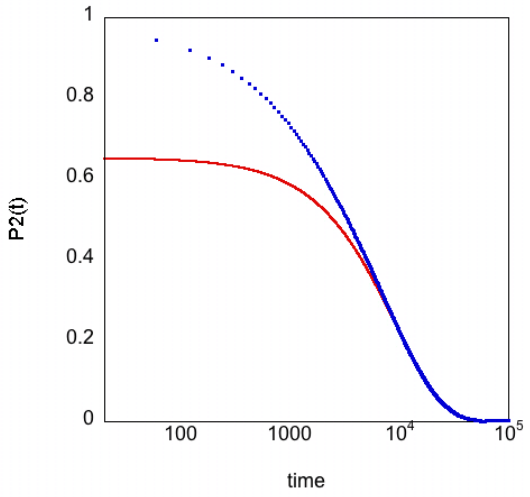

Figure 28: Final Fit of Tail Region

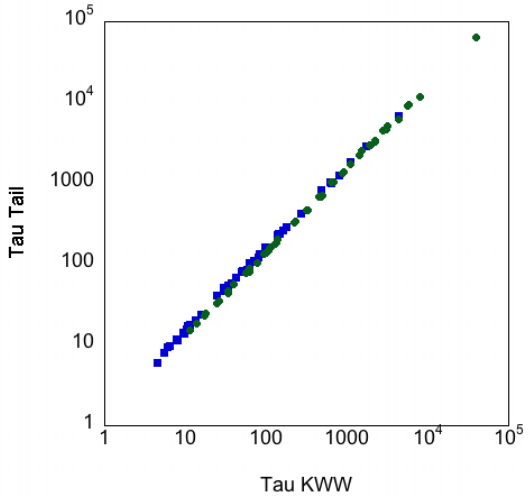

Figure 29: Comparison of τ_{tail} and τ_{KWW}

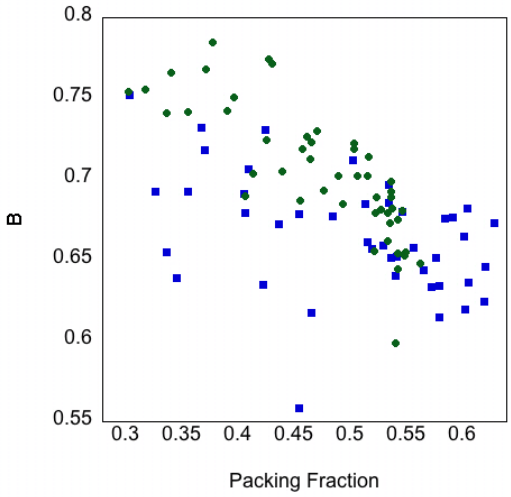

Figure 30: Long-time single exponential constant, B,versus packing fraction

of both the data and our piecewise construction and overlay the two transformed functions. To avoid introducing error associated with a numerical derivative one utilizing the following property:

$$\mathcal{L}\left(-\frac{d\phi\left(t\right)}{dt}\right)=\imath\omega\mathcal{L}\left[\phi\left(t\right)\right]-\phi\left(0\right) \tag{61}$$

An example overlay for the transformed data and fit for the imaginary part of the transform is shown in figure 31. The result is fairly good but it but can be improved by patching the long-time region of the P_2 function with the obtained single-exponential fit instead of truncating the curve. The patch is begun where the function begins to become noise limited ($P_2\left(t\right)\approx 0.10\rightarrow 0.05$) to attempt an limit the amount of bias introduced into the transform. The result is much nicer as is seen in figure 32. The obvious consequence is that we have made an assumption about the long-time behavior of the relaxation function. As the low-frequency (and thus long-time) region of the patched and non-patched transform seem to agree it is clear that we have not introduced much bias.

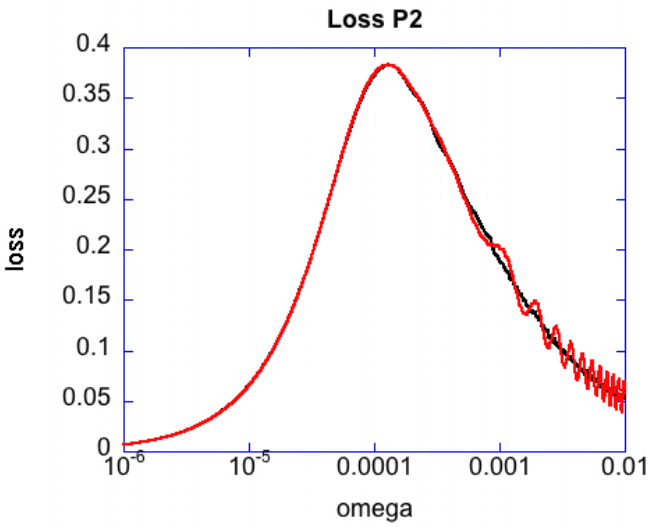

Figure 31: Overlay of Loss P_2

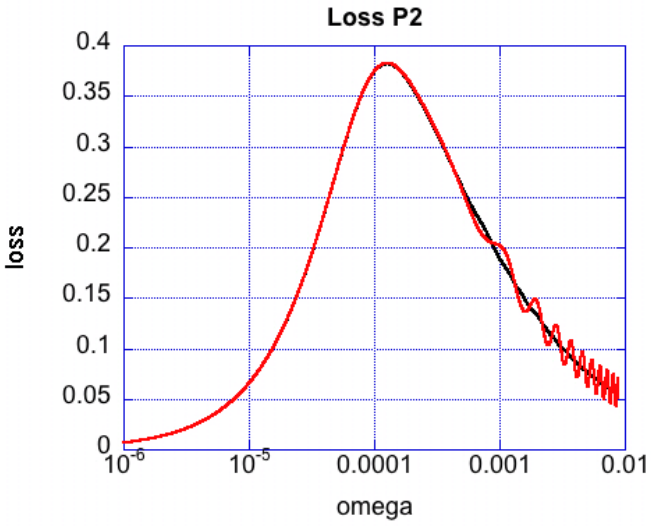

Figure 32: Overlay of Patched Loss P_2

Unfortunately, there appears to be a fair amount of high frequency oscillation in the transformed time-space fit. This is a result of the inexact crossover from the stretched exponential to the single exponential tail introducing a discontinuity into the curve. The discontinuity could be avoided if the continuity of the cross-over point is somehow factored into the fitting procedure or perhaps introducing some smooth interpolant inbetween the two behavior regions. However, we are concerned primarily with producing good parameter values and not so much with the exact transform of our fit.

5.4 The Cole-Davidson Model

5.4.1 Transforming the Data and Time-Temperature Superposition

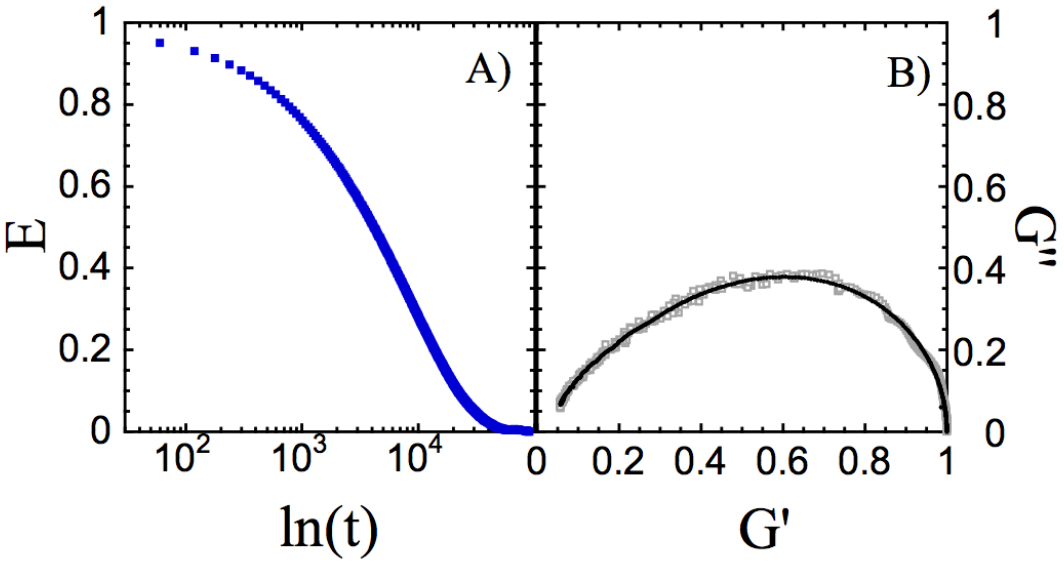

Figure 33: A) P_2 function for an FR system of temperature 1.6 and density 1.06. B) The transform of the P_2 function for the same system. The non-patched data are the noisy grey squares while the patched in the smooth black line

The Cole-Davidson functional form was evaluated by using the same one-sided Fourier transform of the data described in equation (60). In actually performing the transform of the time-dependent data one must cautiously weigh the consequences of truncation. The area of the data as it approaches zero becomes dominated by high-frequency noise which one does not wish to include but one also does not wish to introduce truncation error either. The approach used for these data sets was to use the long-time single exponential fit found earlier to "patch" the long-time region of the relaxation function and effectively remove this high-frequency noise without sacrificing the character of the long-time tail. In figure 33 one can see an example of this transform for a FR system with and without the patch. It is clear that the inclusion of the patch smoothes the curve while retaining the fundamental shape.

One can attempt to apply TTS to the frequency data as was attempted with the time domain data (figure 34). One can see that the loss functions seem to overlay very well on a log-log scale but the differences become very clear when one, instead, plots the data on a linear-log scale.

The inapplicability on TTS to this dataset becomes even more apparent when using a Cole-Cole (CC) [21] plot (see figure 35). One can see that the various curves differ significantly when plotted in this manner and they seem to be qualitatively similar to the CD function.

The reader may notice that many of the curves in figure 3 appear to cross the y-axis while the function forms seem to approach the origin tangent to the y-axis. This y-axis crossing behavior is actually expected for realistic systems and also occurs in the Debye model when molecular inertia is accounted for [70]. The derivation of this expectation follows from the assumption that for a realistic relaxating system the time-dependent relaxation function must have a slope of zero at time zero.

5.4.2 Cole-Davidson Fitting

After performing the transform one then fits the CD function by reducing it into real and imaginary parts obtaining:

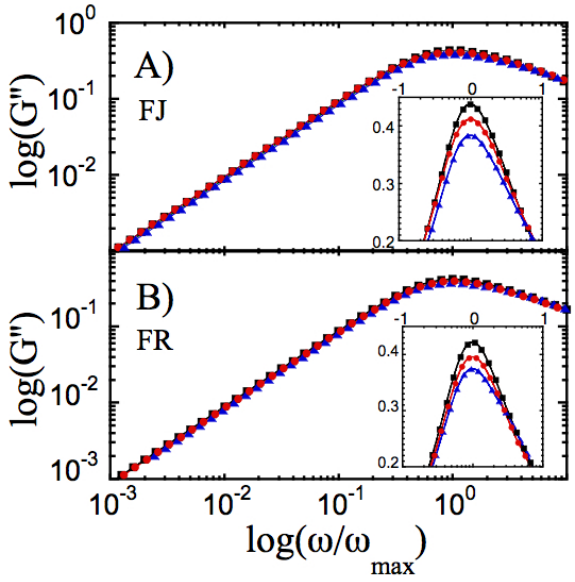

Figure 34: A) Attempted overlay of loss functions for repulsive FJ systems (T,ρ,η): (1.8, 0.593, 0.3037),(1.8, 0.676, 0.3462) and (0.5, 1.06, 0.6207) (black squares, red circles and blue triangles). The insert is a close up of the peak on a linear-log scale. B) Same as A but attempted for repulsive FR systems (1.6, 0.6123, 0.318), (2.0, 0.944, 0.477) and (1.6, 1.06, 0.5633) (black squares, red circles and blue triangles)

$$\left(\frac{1}{1+\imath\omega\tau}\right)^{\beta} = \cos\beta\Theta\cos^{\beta}\Theta - \imath\sin\beta\Theta\cos^{\beta}\Theta \tag{62}$$

where:

$$\Theta = \arctan\omega\tau \tag{63}$$

Then one can either fit the real and imaginary parts simultaneously or separately again using a nonlinear least squares algorithm. The section of the curve near the Nyquist cut-off, $\omega = \pi\Delta t$, was not used in the fits as the error due to finite sampling begins to dominate the behavior of the transform in that region. The separate fits are shown in figures 36 and 37.

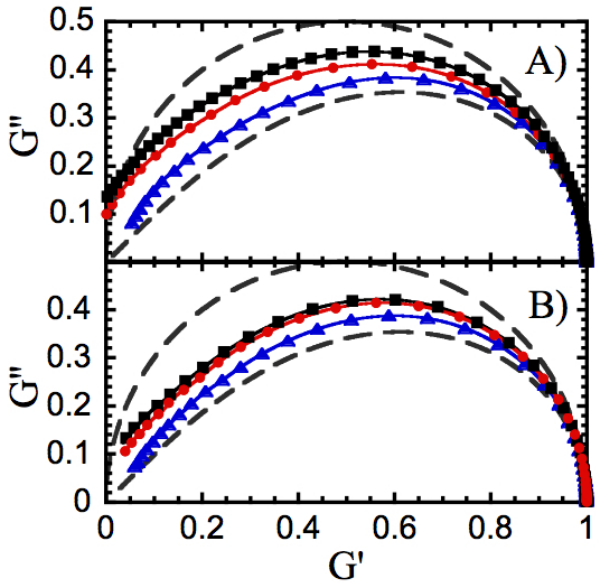

Figure 35: A) CC plots for FJ systems (T,ρ,η): (1.8, 0.593, 0.3037)-R,(1.8, 0.676, 0.3462)-R and (0.5, 1.06, 0.6207)-R (black squares, red circles and blue triangles). The insert is a close up of the peak on a linear-log scale. B) Same as A but for FR systems (1.6, 0.6123, 0.318)-R, (2.0, 0.8056, 0.407)-R and (0.8, 0.944, 0.552)-A (black squares, red circles and blue triangles). The dashed lines correspond to the Debye function and a CD function of β=0.5

These fits appear to work fairly well. However, they are shown using a logarithmic x-axis which sometimes makes the fits look better than they really are. In figure 38 we see that the CD function does not exactly describe the location and shape of the peak in the loss modulus.

However, there may not exist any simple functional forms that could perform any better. Fits of the more complicated Havriliak-Negami form were attempted:

$$\frac{G(\omega)^* - G_\infty}{G_0 - G_\infty} = \left(\frac{1}{1 + (\imath\omega\tau_{CD})^\alpha}\right)^{\beta_{CD}} \tag{64}$$

and the additional parameter, α, converged to a value of one and thus corre-

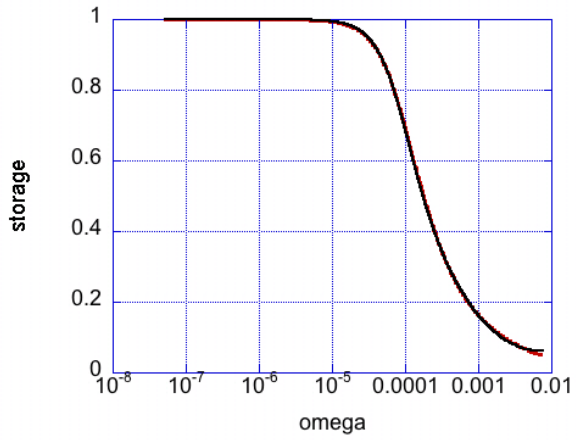

Figure 36: LM fit of Real Part of Transform

sponded to the CD form. Regardless, the CD function seemed to perform to a satisfactory level across a wide range of state points for both FR and FJ systems (see figure 39).

Applying this fitting procedure to the same systems as used for the KWW fitting one obtains the relationships with packing fraction seen in figure 40.The reported values of β_{CD} and τ_{CD} are the average of those obtained from fitting the real and imaginary parts. It was found that the behavior of β_{CD} with respect to η very closely mirrors that of β_{KWW} as is seen in figures 40A and 40C. Both methods result in a collapse of the parameter, β, with regard to packing fraction.

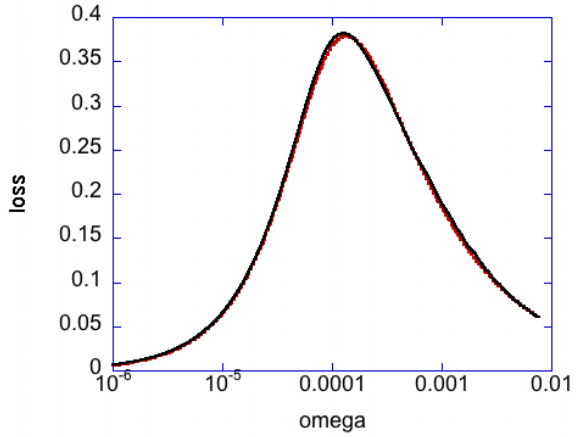

Figure 37: LM fit of Imaginary Part of Transform

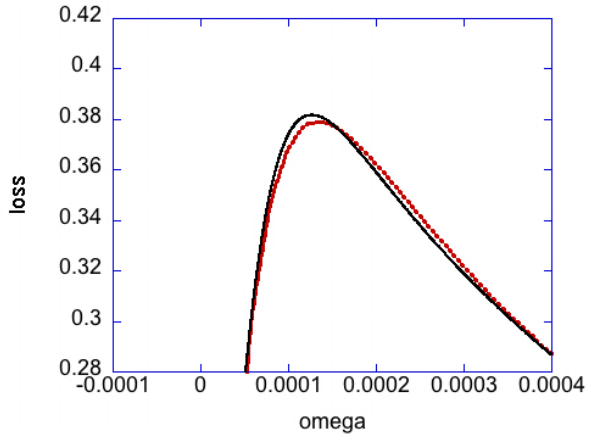

Figure 38: Closeup of LM fit of Imaginary Part of Transform

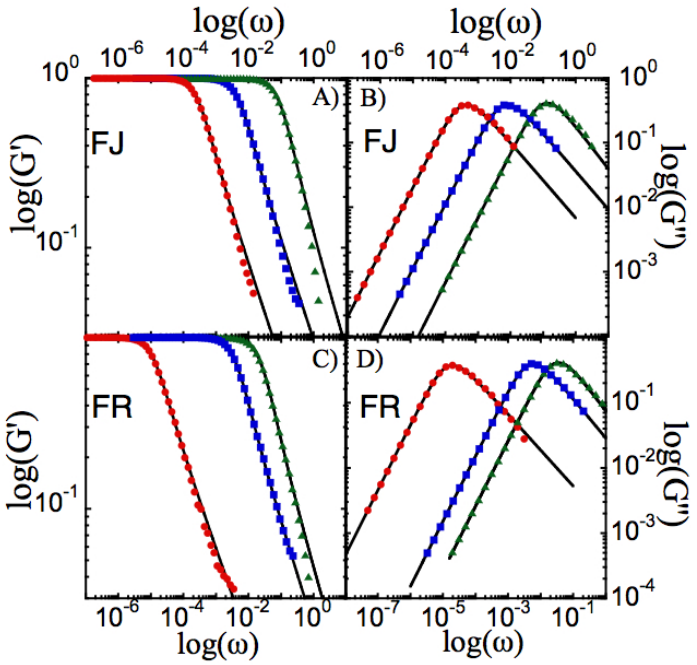

Figure 39: A) and B) Storage and loss plots for repulsive FJ systems with CD fits (T,ρ,η,β,τ): (0.5, 1.06, 0.621, 0.575, 3544.5),(1.0, 1.033,0.566, 0.581, 196.56) and (1.8, 0.676 0.3462, 0.6508, 10.494) (red circles, blue squares and green triangles). C) and D) Same for FR systems: (1.6, 1.06, 0.5633, 0.545, 83720)-A, (2.0, 0.944, 0.477, 0.606, 10.35)-R and (1.2, 0.6628, 0.356, 0.662, 39.61)-R

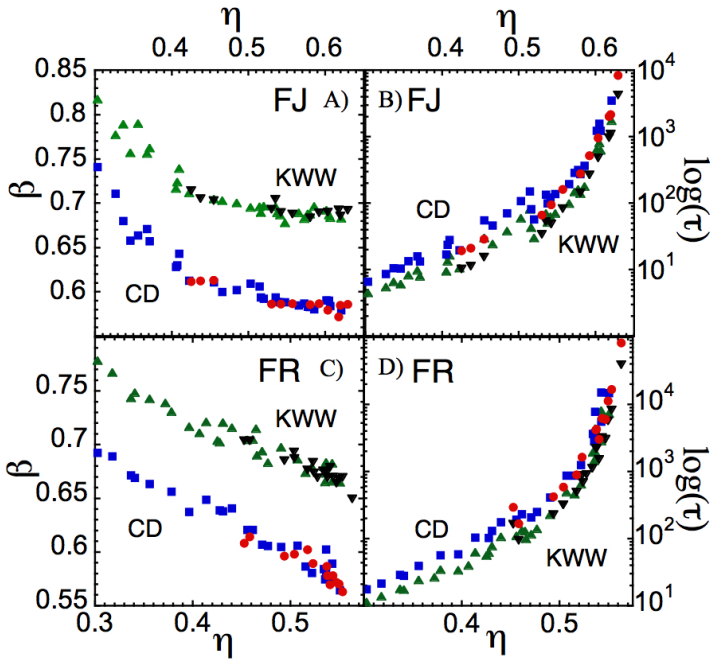

Figure 40: A) Obtained s for FJ systems. The solid green triangles and inverted black triangles represent KWW fits for repulsive and attractive systems respectively. The solid blue squares and red diamonds represent CD fits for repulsive and attractive systems respectively. B) The obtained s for the same FJ systems using same labeling scheme as A. C) Obtained s for FR systems using the same scheme as A. D) The obtained s for the same FR systems using same labeling scheme as A.

5.4.3 Comparison of the CD and KWW forms

At first glance it appears that the two functions merely differ by some constant. In fact, the relationship between β_{CD} and β_{KWW} is found to be linear (figure 41A) for FR and FJ systems. The relationships obtained by least squares fitting were:

$$\beta_{KWW} = 0.747\beta_{CD} + 0.253 \tag{65}$$

for FJ systems and:

$$\beta_{KWW} = 0.778\beta_{CD} + 0.223 \tag{66}$$

for FR systems. The fits were regularized by taking advantage of the fact that for $\beta_{CD} = 1$ the curve is a Debye function and therefore it is required that $\beta_{KWW} = 1$ as well. These relationships differ from the one found by Lindsey and Patterson [50] (solid line in figure 6A):

$$\beta_{KWW} = \begin{cases} 0.970\beta_{CD} + 0.144 & 0.2 \leq \beta_{CD} \leq 0.6 \\ 0.683\beta_{CD} + 0.316 & 0.6 \leq \beta_{CD} \leq 1.0. \end{cases} \tag{67}$$

It is possible that this difference reflects the fact that our relaxation functions were not found to be globally described by a KWW function but rather only in a small intermediate region in time.

A similar correlation between the KWW and CD functions was found for the decay constants τ_{KWW} and τ_{CD} (figures 40B and 40D). The relationship (figure 6B) between τ_{KWW} and τ_{CD} was found to be:

$$\tau_{KWW} = \tau_{CD}(1.1877\beta_{CD} - 0.1877) \tag{68}$$

$$\tau_{KWW} = \tau_{CD}(1.141\beta_{CD} - 0.141) \tag{69}$$

for FJ and FR systems respectively. Again the least squares fits were regularized by applying the constraint that when the curve is a Debye function, $\beta_{CD} = \beta_{KWW}$, then it is required that τ_{CD}= τ_{KWW} . The Lindsey-Patterson prediction for the decay constant seems reasonable for FJ systems but not

for FR systems:

$$\tau_{KWW} = \tau_{CD}(1.184\beta_{CD} - 0.184) \tag{70}$$

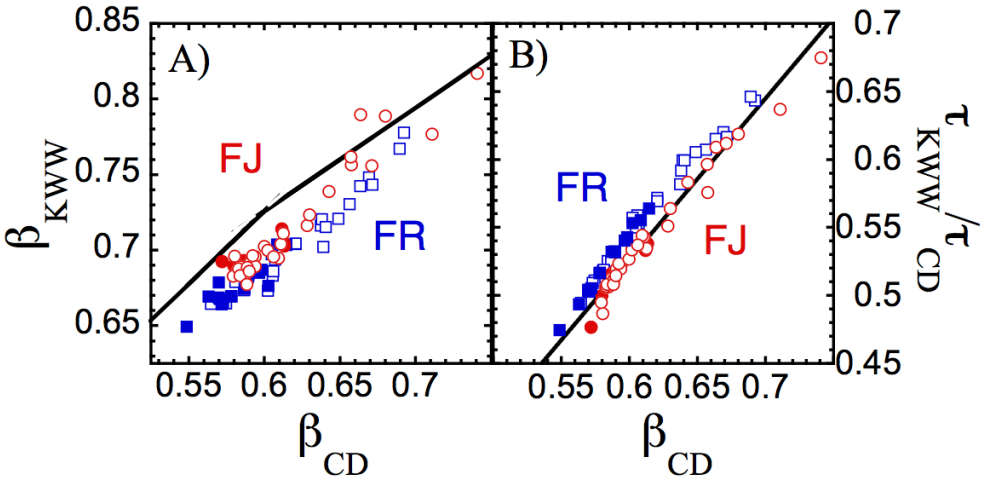

Figure 41: A) Cross-plot of βs obtained through KWW and CD fits of the data. The solid red circles correspond to FJ-attractive and the hollow to FJ-repulsive. The solid blue squares correspond to FR-attractive and the hollow to FR-repulsive. The solid line corresponds to the relationship found by Lindsey and Patterson. B) Cross-plot of τ obtained through KWW and CD fits of the data. The solid line is the predicted relationship by Lindsey. The solid red circles correspond to FJ-attractive and the hollow to FJ-repulsive. The solid blue squares correspond to FR-attractive and the hollow to FR-repulsive.

The difference between the mappings of the CD relaxation parameters to those of the KWW function for each system is not altogether unexpected and may possibly indicate variation in the composition of the relaxation functions for the systems (FJ and FR) and/or some difference in descriptive bias between the two functional forms (KWW and CD).

5.4.4 Discussion

The decision of which functional form one should use to describe relaxation phenomena is not one to be taken lightly. The behavior of the various functions are actually quite different when the underlying distributions of relaxations times are studied [38, 81]. It has been found that one type of representation of relaxation can often be adequately described by another for certain parameter and frequency ranges [50, 78, 6, 7, 35] however the commonly found mappings from one function to another can be inaccurate in other instances [38]. The KWW function is very often used due to the lack of competing time-space functions that describe relaxation. As is clear from the above sections, the KWW function does not seem to be as practical as the CD function in describe the decay of the end to end vector. Describing the intermediate to long regions of this decay in time required the use of both a KWW and single exponential function and a total of six parameters. The CD function appears to achieve a high quality fit in frequency using only two. Using the inverse transform [88, 50]:

$$P_2(t) = \int_0^\infty \frac{G''(\omega)}{G_0 - G_\infty} \cos \omega t \frac{d\omega}{\omega} \tag{71}$$

where $G_0 - G_\infty$ is chosen as to normalize the result and applying this transform to the CD fit (figure 42) one can see the CD function works surprisingly well in time space.

In figure 42 the fits of the KWW and CD functions for a sample E(t) are compared both in time and by using a CC plot. It can be seen that these two fits describe very different regions of the decay function. The KWW functions seems more appropriate in the short to intermediate time regions while the CD function fits much better for the intermediate to long time domain. The KWW function could, of course, be fit a number of other ways (figure 43) however, as was shown earlier, the fitting would be performed over the wrong region. It also becomes clear from figure 42 and 43 that without using additional terms (such as a single exponential) the frequency spectrum will not be adequately fit by a KWW function. In the context of our previous findings, it is surprising that such a good fit of the data is obtained using only the CD function. The underlying distribution of relaxation times (figure 14) of the CD function increases rapidly and then displays a sharp cut-off

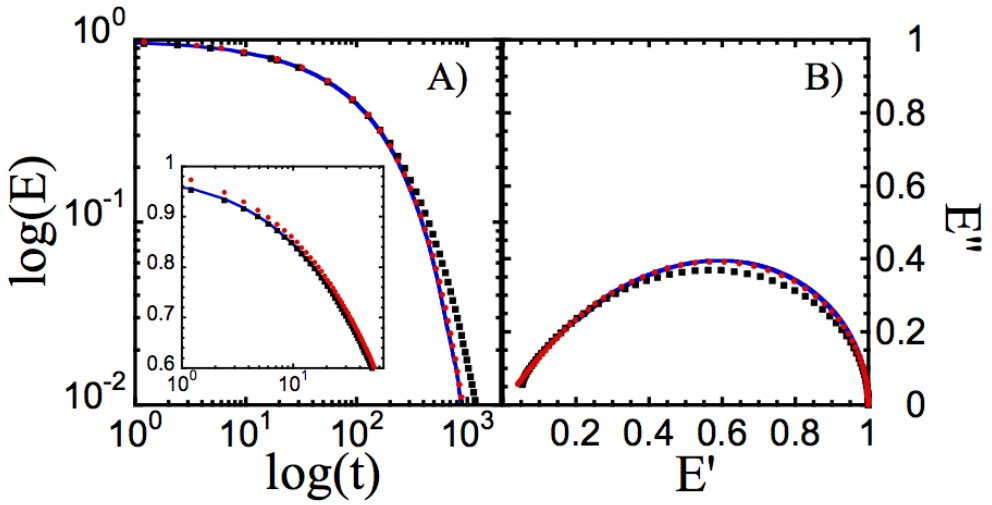

Figure 42: A) Comparison of KWW fit (dotted black line) as calculated by the method of section 5.3.3 and the inverse transform of the CD fit (dotted red line) of a repulsive FR system (T=2.0, ρ=0.944, η=0.477). The original data corresponds to the solid blue line. The insert is a close-up of the short time region to emphasize the difference between the KWW and CD fits in this region. B) Comparison of transformed KWW and CD function fits plotted in a Cole-Cole fashion using the same color scheme as part A.

at large times while the distribution for the KWW function slowly decays to zero at large relaxation times. The sharp cut-off present in the distribution for the CD function ensures that there exists a well defined largest relaxation time, in other words, a single exponential tail.

The differences in the descriptive bias of the KWW and CD functions are made even more clear when one attempts to map the parameters of one function to another in spite of the discrepancy between the underlying distributions of relaxation times. Many such attempts exist in the literature [50, 74, 91] however the obtained mappings almost always differ from each other to some significant extent. This lack of correspondence is likely due to differences in fitting procedure and/or, if the map is attempted through experimental or simulation data, the fact that the underlying data is not likely to be perfectly described by either or both of the functions over their

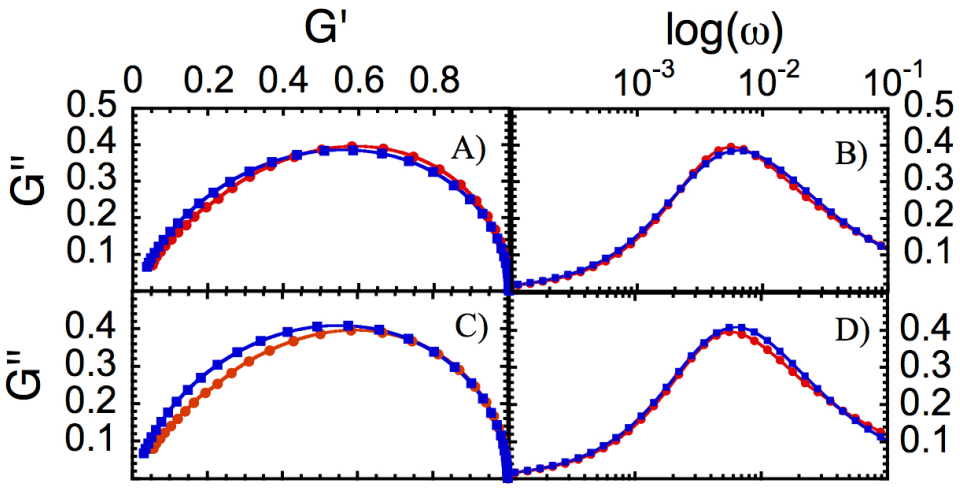

Figure 43: A) Cole-Cole plot of the transformed data (red circles) and transform of KWW function (blue squares) using parameters predicted from LP and the obtained CD parameters. B) Corresponding losses for fit in part A. C) Cole-Cole plot of transformed data (red circles) and transform of KWW function (blue squares) using parameters which provide and excellent fit of the low frequency regions. D) Corresponding loss plots for fit in part C.

entire domains. It has been seen in earlier sections and [9] that the KWW function parameters can be very sensitive to the manner to which they are obtained. These details in the fitting procedure may not have been adequately addressed in previous comparisons of the KWW and CD functions.

5.5 Torsional Systems

The results of CD fit are promising, however, we have only considered the FR and FJ models thus far. The addition of a torsional barrier to the dihedral angles of the simulated chains greatly complicates matters. Two relaxation functions, the P_2 and DACF, must be dealt with. Recalling section 1.3 we know the magnitude of the peaks of the torsional barrier to coincide with a temperature of 2.8 in Lennard-Jones units. It was found for temperatures greater than approximately 2.0 that the systems did not differ in overall

behavior significantly from the FR systems. Packing fraction functioned reasonably well as a scalar metric for the diffusion coefficient and the DACF curves decayed very quickly compared with the P_2 function. However, as one approaches lower temperatures the situation is very different.

5.5.1 Diffusion and the Scalar Metric

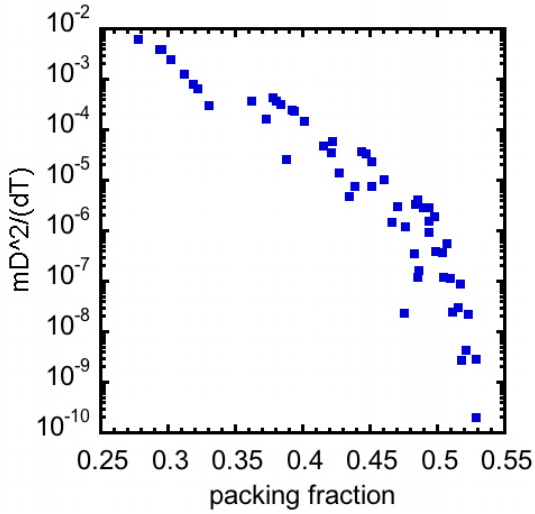

Figure 44: The square of D^* versus η for repulsive Torsion systems. One can see the beginnings of separate density lines in stark contrast to the smooth single-valued function that existed for FR and FJ systems (see figure 9)

For the FR and FJ systems the work of finding a suitable scalar metric was primarily the work of former students [18, 36]. Their results functioned as a foundation from which the chain relaxation could be explored and then compared to. Unfortunately, for systems with torsional barriers packing fraction ceased to be a suitable scalar metric. In figure 44 one can see this breakdown occurring.

One witnesses the beginnings of individual curves for each density form as the temperature decreases significantly below 2.0. As a result it was decided to follow the method of Casalini and Roland [20] in which one uses the following collapse function:

$$C = T^{-1}V^{-\gamma} = \frac{\rho^{\gamma}}{T} \tag{72}$$

where V is the specific volume and γ is a material dependent constant. The parameter, γ is generally obtained via trial and error. In figure 45 one can see the result of this procedure applied to D^*.

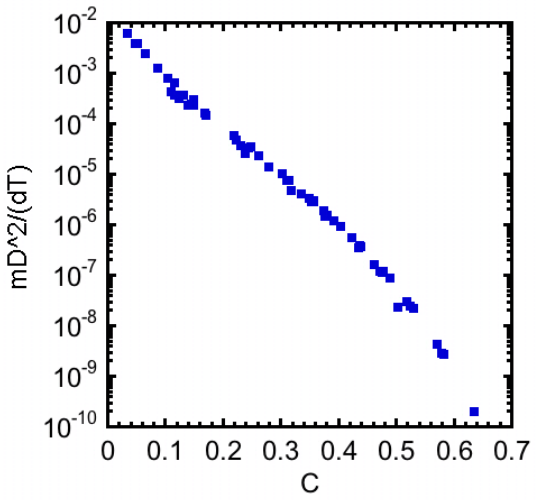

Figure 45: The square of D^* versus $\frac{\rho^{4.15}}{T}$ for repulsive Torsion systems.

It is easily seen that this result is much cleaner than the one obtained using packing fraction. The same procedure can be applied to other dynamic quantities for which, in general, the value of γ will differ. It is unfortunate that this is the case because one is thus required to collect a number of γ values to describe a single material.

5.5.2 P_2 and the DACF

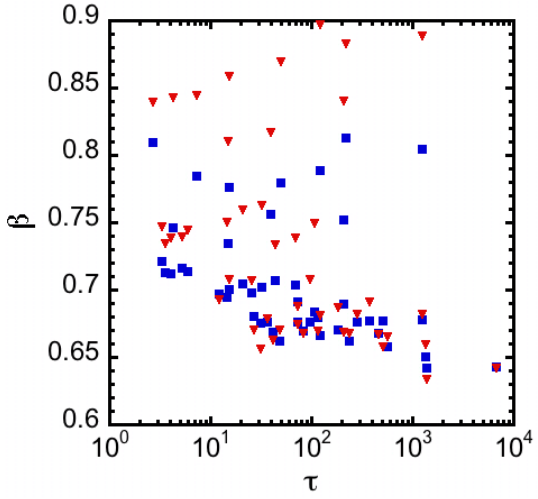

Figure 46: β versus τ for repulsive Torsion systems. The squares correspond to the P_2 function and the inverted triangles to the DACF

Not only for the diffusion coefficient did the addition of torsional barriers complicate matters. In dealing with the relaxation functions not only was packing fraction unavailable as a scalar metric but the parameters of these functions also ceased to be single valued functions of the decay constant τ. The P_2 and DACF were both fitted using the procedure outlined for the FR and FJ data. The stretching exponent, β was a function of both τ and T (figure 46).

Even the relationship between the decay constant of the P_2 function and the DACF is not a simple matter. As the temperature of the system is decreased the DACF begins to decay much more slowly than the P_2 function resulting in the DACF becoming the limiting relaxation process. Applying the CR procedure to β one obtains the result in figure 47

A reasonable collapse is thus obtained. However, one begins to wonder that

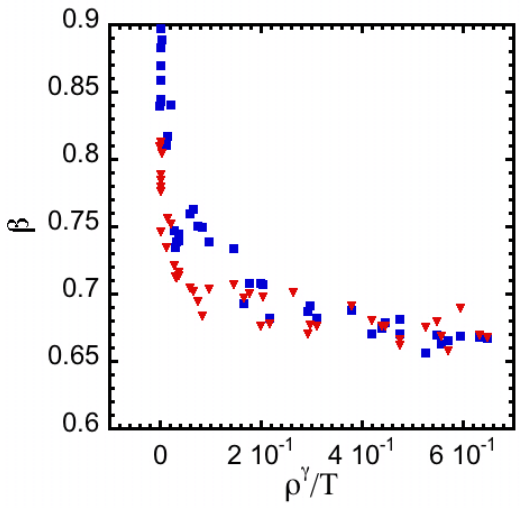

Figure 47: β versus $\frac{\rho^{11}}{T}$ for repulsive Torsion systems. The squares correspond to the P_2 function and the inverted triangles to the DACF

when using such a large value of γ whether the collapse function is really physically relevant. One could, for example, be merely plotting the data in such a way that the differences between the points are made only to look less significant. Without any tie to a physical theory it is difficult to know. The procedure is applied to the decay constants in figure 48. In this plot one sees that a collapse of τ for the DACF with regard to the CR collapse function does not seem possible. It is clear that a great deal more work will be necessary in the search for a scalar metric for this data.

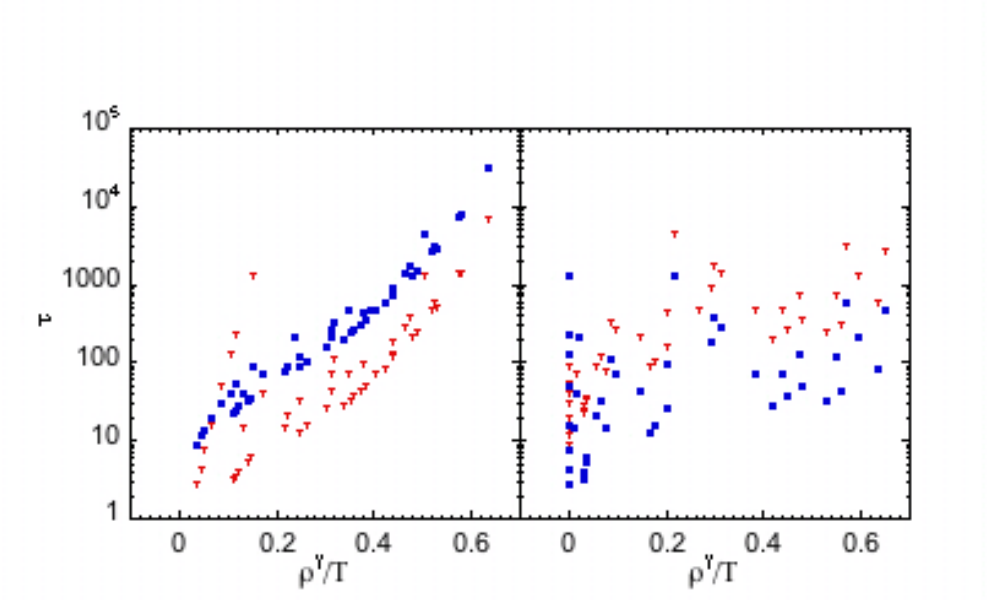

Figure 48: Left) τ versus $\frac{\rho^{4.15}}{T}$ for repulsive Torsion systems. The squares correspond to the P_2 function and the inverted triangles to the DACF Right) τ versus $\frac{\rho^{11}}{T}$

6 Conclusions

There are several important messages to be extracted from the body of work presented in this paper. Some of these messages pertain to the specifics of the results and others, more general, which pertain to the field as a whole. It is hoped that from the results section the difficulty of extracting useful information from relaxation functions is clear. In dealing with data that does not contain distinguishing landmarks it is not easy to know when differences in the data become significant or whether one is analyzing the correct region. Additionally, it becomes apparent that a more consistent theory of relaxation in disordered materials is necessary to make the analysis of such materials both more practical and more applicable to reality.

The need for such a theory is most evident when attempting to fit P_2 functions or the DACF where one is required to make use of empirically based fitting functions. The use of the KWW function posed several difficulties because of the fact that the function only applies in a narrow region. While the methodology presented above renders the determination of this region much easier than it was before one is still required to piece together several functions to describe a single continuous curve.

With the CD function, on the other hand, one is able to almost completely describe the relaxation using only two parameters. However, unless one performs their simulation or experiment in the frequency domain one is faced with the difficult task of transforming the data. One must balance many requirements to successfully transform the data. One wishes to eliminate noise without altering the fundamental character of the data.

Several options exist for dealing with this issue. One could truncate and risk losing important data, smooth and risk significantly altering the data's character or having to dedicate greater amounts of time in collecting the data in order to reduce the influence of noise. Fortunately for the FR and FJ and some of the torsion systems the single exponential "tail" of the relaxation function could be used to smooth only the last region of the data where the amplitude of the noise becomes greater than that of the signal. However, it was found to be impossible to determine the the single exponential region for many of the DACFs obtained from high temperature Torsional systems.

There were other difficulties in analyzing the Torsional model that did not exist for the FR and FJ models. All of the assumptions that could be used for the simpler molecular models were clearly not applicable. A suitable scalar metric could be found for individual relaxation parameters but no scalar metric could be found to be universally applicable and in the case of τ_{DACF} no such metric could be discovered. Clearly a new approach will be necessary to remedy this problem.

The completion of the above work was no trivial matter. In simulation research the data gathering process can be very long and tedious. In contrast to a great deal of experimental research the costs associated with this data gathering process lies only with time and manpower. Without the limitation of having to buy expensive materials to perform the research on or new expensive equipment whenever one seeks to explore a new aspect of the research the expectations on the quality of the data thus becomes much more stringent. While only about one hundred unique data points are shown in the above plots each point represented tens of hours of work. Data for a single state point would often be rerun several times as ever higher standards of precision became necessary. Additionally, several different methods would often be explored simultaneously each with their own requirements from the data.

The field of this research requires a great deal of background knowledge that one is generally unlikely to encounter in the course of one's undergraduate education. Making sense of all of it can seem to be an insurmountable task and it often easy to lose sight of the big picture. It is hoped that this paper will serve not only as a review of all the work performed for the last year and a half but also as a useful guide for those beginning work in closely related areas.

References

[1] K. Adachi, H Yoshida, F Fukui, and T Kotaka. Comparison of dielectric and viscoelastic relaxation spectra of polyisoprene. *Macromolecules*, pages 3138–3144, 1990.

[2] D.B. Adolf, R.S. Chambers, J. Flemming, J. Budzien, and J. McCoy. Potential energy clock model: Justification and challenging predictions. *Journal of Rheology*, 51(3):517–540, 2007.

[3] O. Ahumada, D.N. Theodorou, A. Triolo, V. Arrighi, C. Karatasos, and J.-P. Ryckaert. Segmental dynamics of atactic polypropylene as revealed by molecular simulations and quasielastic neutron scattering. *Macromolecules*, 35(18):7110–7124, 2002.

[4] M.P. Allen and D.J. Tildesley. *Computer simulation of liquids*. Oxford University Press, 1989.

[5] D. Alvarez, S. Franz, and F. Ritort. Fragile-glass behavior of a short-range p-spin model. *Physical Review B*, 54(14), 1996.

[6] F. Alvarez, A. Alegra, and J. Colmenero. Relationship between the time-domain kohlrausch-williams-watts and the frequency-domain havriliak-negami relaxation functions. *Physical Review B*, 44(14):7306–7312, 1991.

[7] F. Alvarez, A. Alegra, and J. Colmenero. Interconnections between frequency-domain havrilliak-negami and time-domain kohlrausch-williams-watts relaxation functions. *Physical Review B*, 47(1):125–130, 1993.

[8] D.V. Anosov. Ergodicity of a dynamical system. In Michiel Hazewinkel, editor, *Encyclopedia of Mathematics*. Kluwer Academic Publishers, 2002.

[9] D. Apitz and P.M. Johansen. Limitations of the stretched exponential function for describing dynmaics in disordered solid materials. *Journal of Applied Physics*, 97(6):063507, 2005.

[10] G. Arialdi, K. Karatasos, J.-P. Ryckaert, V. Arrighi, F. Saggio, A. Triolo, A. Desmedt, J. Pieper, and R.E. Lechner. Local dynamics of polyethylene and its oligomers: A molecular dynamics interpretation of the in-

coherent dynamic structure factor. *Macromolecules*, 36(23):8864–8875, 2003.

[11] R. Aster, B. Borchers, and C. Thurber. *Parameter Estimation and Inverse Problems*. Elsevier Academic Press, 2004.

[12] J.A. Barker and D. Henderson. Pertubation theory and equation of state for fluids ii. a successful theory of liquids. *The Journal of Chemical Physics*, 47(11), 1967.

[13] U. Bengtzelius, W. Gotze, and A. Sjolander. Dynamics of supercooled liquids and the glass transition. *Journal of Physics C: Solid State Physics*, 17:5915–5934, 1984.

[14] C. Bennemann, J. Baschnagel, and W. Paul. Molecular-dynamics simulation of a glassy polymer melt: Incoherent scattering function. *The European Physics Journal B*, 10:323–334, 1999.

[15] H.J.C Berendsen and et al. Molecular-dynamics with coupling to an external bath. *Journal of Chemical Physics*, 81(8):3684–3690, 1984.

[16] Ann-Charlotte Berglund. Tikhonov regularization with linear inequality constraints, June 1999.

[17] R.K. Bharadwaj and R.H. Boyd. Effects of pressure on conformational dynamics in polyethylene: A molecular dynamics simulation study. *Macromolecules*, 33:5897–5905, 2000.

[18] J. Budzien, J.D. McCoy, and D.B. Adolf. General relationships between the mobility of a chain fluid and various computed scalar metrics. *Journal of Chemical Physics*, 121(20), 2004.

[19] H.B. Callen and T.A. Welton. Irreversibility and generalized noise. *Physical Review*, 1951.

[20] R. Casalini and C.M. Roland. Thermodynamical scaling of the glass transistion dynamics. *arXiv:cond-mat/0403622v1*, 2003.

[21] K.S. Cole and R.H. Cole. Dispersion and absorption in dielectrics i. alternating current characteristics. *Journal of Chemical Physics*, 9(4), 1941.

[22] J. Colmenero, A. Alegria, J.M. Alberdi, and F. Alvarez. Dynamics of the α relaxation of a glass-forming polymeric system: Dielectric, mechanical, nuclear-magnetic-resonance, and neutron-scattering studies. *Physical Review B*, 44(14), 1991.

[23] Charles Daniels. Polymer glass transition. Case Western Reserve. Geon Corp. http://plc.cwru.edu/tutorial/enhanced/files/polymers/therm/therm.htm.

[24] D.W. Davidson and R.H. Cole. Dielectric relaxation in glycerol, propylene glycol, and normal-propanol. *Journal of Chemical Physics*, 19(12):1484–1490, 1951.

[25] Peter Debye. *Polar Molecules*. Dover, 1929.

[26] M. Doi and S.F. Edwards. *The Theory of Polymer Dynamics*. International Series of Monographs on Physics - 73. Clarendon Press, Oxford, 1988.

[27] M.D. Ediger. Spatially heterogeneous dynamics in supercooled liquids. *Annu. Rev. Phys. Chem.*, pages 99–128, 2000.

[28] A. Feltz. *Amorphous Inorganic Materials and Glasses*. Weinheim/VCH, 1993.

[29] J.D. Ferry. *Viscoelastic Properties of Polymers*. John Wiley and Sons, 1980.

[30] Gordon S. Fulcher. Analysis of recent measurements of the viscosity of glasses. *Journal of the American Ceramic Society*, 8(6):339–355, 1925.

[31] W. Gotze and L. Sjogren. Relaxation processes in supercooled liquids. *Reports on Progress in Physics*, 55(3), 1992.

[32] G.S. Grest and K. Kremer. Molecular-dynamics simulation for polymers in the presence of a heat bath. *Phys. Rev. A*, 33(5):3628–3631, 1986.

[33] V. Halpern. Nonexponential relaxation and fragility in a model system and in supercooled liquids. *The Journal of Chemical Physics*, 124, 2006.

[34] J.P. Hansen and I.R. McDonald. *Theory of Simple Liquids*. Academic Press, 2nd edition, 1986.

[35] S. Havriliak and S.J. Havriliak. Comparison of the hariliak-negami and stretched exponential functions. *Polymer*, 37(18):4107–4110, 1996.

[36] J.V. Heffernan, J. Budzien, A.T. Wilson, R. Baca, V.J. Aston, F. Avila, and D.B. Adolf. Molecular flexibility effects upon liquid dynamics. *Journal of Chemical Physics*, 126, 2007.

[37] A. Heuer and H.W. Spiess. Comment on "dynamics of glass-forming polymers: 'homogeneous' versus 'heterogeneous' scenario". *Physical Review Letters*, 82(6):1335, February 1990.

[38] R. Hilfer. H-function representations for stretched exponential relaxation and non-debye susceptibilities in glassy systems. *Physical Review E*, 65(6):061510, 2002.

[39] PSP Inc. Elastomer properties - stress relaxation/retained sealing force. http://www.pspglobal.com/properties-stress-relaxation.html.

[40] A.A. Istratov and O.F. Vyvenko. Exponential analysis in physical phenomena. *Review of Scientific Instruments*, 70(2):1233–1257, 1999.

[41] G.P. Johari. Intrinsic mobility of molecular glasses. *Journal of Chemical Physics*, 58:1766–1770, 1973.

[42] K. Karatasos and D.B. Adolf. Slow modes in local polymer dynamics. *Journal of Chemical Physics*, 112(19):8225–8228, 2000.

[43] K. Karatasos, D.B. Adolf, and S. Hotston. Effects of density on the local dynamics and conformational statistics of polyethylene: A molecular dynamics study. *Journal of Chemical Physics*, 112(19):8695–8706, 2000.

[44] F. Kohlrausch. Über die elastische nachwirkung bei der torsion. *Poggendorff's Annalen der Physik*, 119:337–368, 1863.

[45] K. Kremer and G.S. Grest. Molecular dynamics (md) simulations for polymers. *Journal of Physics: Condensed Matter*, pages SA295–SA298, 1990.

[46] R Kubo. The fluctuation-dissipation theorem. *Reports on Progress in Physics*, 29(1):255–284, 1966.

[47] R.G. Larson. *The Structure and Rheology of Complex Fluids*. Oxford University Press, 1999.

[48] E. Leutheusser. Dynamical model of the liquid-glass transition. *Physical Review A*, 29(5), 1984.

[49] K. Levenberg. A method for the solution of certain problems in least squares. *Quart. Appl. Math*, 2:164–168, 1944.

[50] C.P. Lindsey and G.D. Patterson. Detailed comparion of the william-watts and cole-davidson functions. *Journal of Chemical Physics*, 73(7):3348–3357, 1980.

[51] P. Lunkenheimer, R. Wehn, U. Schneider, and A. Loidl. Glassy aging dynamics. *Physical Review Letters*, 95, 2005.

[52] M.L. Mansfield. Ising spin glass that closely resembles the physical glass transition. *Physical Review E*, 66, 2002.

[53] N.H. March and M.P. Tosi. *Introduction to Liquid State Physics*. World Scientific, 2002.

[54] D. Marquardt. An algorithm for least-squares estimation of nonlinear parameters. *SIAM Journal of Applied Math*, 11:431–441, 1963.

[55] G.B. McKenna. On the physics required for prediction of long term performance of polymers and their composites. *Journal of Research of the National Institute of Standards and Technology*, 99(2), 1994.

[56] K.L. Ngai. Universality of low-frequency fluctuation, dissipation and relaxation properties of condensed matter. *Comments in Solid State Physics*, 9:127, 1979.

[57] K.L. Ngai. Dynamic and thermodynamic properties of glass-forming substances. *Journal of Non-Crystalline Solids*, 275(1), 2000.

[58] K.L. Ngai. Short-time and long-time relaxation dynamics of glass-forming substances: a coupling model perspective. *Journal of Physics: Condensed Matter*, 12:6437–6451, 2000.

[59] K.L. Ngai. Short-time and long-time relaxation dynamics of glass-forming substances: a coupling model perspective. *Journal of Physics: Condensed Matter*, 2000.

[60] K.L. Ngai and R.W. Rendell. Cooperative dynamics in relaxation: A coupling model perspective. *Journal of Molecular Liquids*, pages 199–214, 1993.

[61] K.L. Ngai, R.W. Rendell, A.K. Rajagopal, S. Teiltler, and S. Ann. Three couple relations for relaxations in complex systems. *N.Y. Acad. Sci.*, 484:150–184, 1986.

[62] V et al Norikov. Nature poisson's ratio and the fragility of glass forming liquids. *Nature*, pages 961–963, 2004.

[63] S. Nose. A molecular-dynamics method for simulations in the canonical ensemble. *Molecular Physics*, 52(2):255–268, 1984.

[64] I Nyquist. Agitation of electric charge in conductors. *Physical Review*, 32(1):110–113, 1928.

[65] T. Pakula. Mechanics, rheology and dielectric spectroscopy laboratories. Institute broschure, Max Planck Institute for Polymer Research, 2000.

[66] M. Paluch, K.L. Ngai, and S. Hensel-Bielowka. Pressure and temperature dependences of the relaxation dynamics of cresolpthalein-dimethylether. *Journal of Chemical Physics*, 114(24), 2001.

[67] J.C. Phillips. Stretched exponential relaxation in molecular and electronic glasses. *Reports on Progress in Physics*, 59:1133–1207, 1996.

[68] D.J. Plazek. Temperature depedence of the viscoelastic behavior of polystyrene. *J. Phys. Chem.*, 69(10):3480–3487, 1965.

[69] S.J. Plimpton. Fast parallel algorithms for short-range molecular dynamics. *Journal of Computational Physics*, 117:1–19, 1995. lammps.sandia.gov.

[70] J.G. Powles. Cole-cole plots as they should be. *Journal of Molecular Liquids*, 56:35–47, 1993.

[71] S.W. Provencher. Contin - a general-purpose constrained regularization program for inverting noisy linear algebraic and integral-equations. *Computer Physics Communications*, 27(3):229–242, 1982.

[72] D.R. Reichman and P. Charbonneau. Mode-coupling theory. *Journal of Statistical Mechanics*, 2005.

[73] William P. Rogers. *Report of the Presidential Commission on the Space Shuttle Challenger Accident*. Government Printing Office, Washington, D.C., 1986.

[74] E. Rossler, K. Borner, J. Tauchert, M. Taupitz, and M. Poschl. Reorientational correlation-functions of simple supercooled liquids as revealed by nmr-studes. *Ber. Bunsen-Ges. Phys. Chem. Chem. Phys.*, 95(9):1077–1084, 1991.

[75] P.E. Rouse. A theory of the linear viscoelastic properties of dilute solutions of coiling polymers. *Journal of Chemical Physics*, 21:1272, 1953.

[76] Michael Rubinstein and Ralpha H. Colby. *Polymer Physics*. Oxford University Press, 2003.

[77] X. Shi, A. Mandanici, and G.B. McKenna. Shear stress relaxation and physical aging study on simple glass-forming materials. *The Journal of Chemical Physics*, 123:174507, 2005.

[78] C.R. Snyder and F.I. Mopsik. Limitations on distinguishing between representations of relaxation data over narrow frequency ranges. *Journal of Applied Physics*, 84(8):4421–4427, 1998.

[79] A.P. Sokolov and Y. Hayashi. Breakdown of time-temperature superposition: From experiment to the couplin model and beyond. *Journal of Non-Crystalline Solids*, 353:3838–3844, 2007.

[80] L.H. Sperling. *Introduction to Physical Polymer Science*. Wiley-Interscience, 2001.

[81] V.A. Stephanovich, M.D. Glinkchuk, and B. Hilczer. Relaxation time distribution function. *Ferroeletrics*, 240(1-4):1495–1505, 2000.

[82] Y.M. Stokes. Flowing windowpanes: fact of fiction? *Proceedings: Mathematical, Physical and Engineering Sciences*, 455(1987):2751–2756, 1999.

[83] K.Y. Tsang and K.L. Ngai. Relaxation in interacting arrays of oscillators. *Physical Review E*, 54(4), 1996.

[84] L. Verlet. Computer "experiments" on classical fluids. I. *Physical Review*, 159(1), 1967.

[85] B. Veytsman and M. Kotelyanskii. Periodic boundaries for off-lattice simulations. http://www.plmsc.psu.edu/ www/matsc597c-1997/simulations/lecture3/node2.html.

[86] Hans Vogel. The law of the relation between the viscosity of liquids and the temperature. *Physik. Z.*, 22:645–646, 1921.

[87] J.D. Weeks, D. Chandler, and H.C. Andersen. Role of repulsive forces in determining the equilibrium structure of simple liquids. *Journal of Chemical Physics*, 54(12), 1971.

[88] G. Williams and D.C. Watts. Non-symmetrical dielectric relaxation behavior arising from a simple empiral decay function. *Transactions of the Faraday Society*, 66:80–85, 1970.

[89] Clare Yu. Glasses: Very sluggish liquids or real solids? *UCI Physics Newsletter*, 5, 1998.

[90] E.D. Zanotto. Do cathedral glasses flow? *American Journal of Physics*, 66(5):392–395, 1998.

[91] M.D. Zeidler. The tricomi time correlation function. *Ber. Bunsen-Ges. Phys. Chem. Chem. Phys.*, 95(9):971–976, 1991.